R. & M. No. 2993
(17,465)
A.R.C. Technical Report



MINISTRY OF SUPPLY

AERONAUTICAL RESEARCH COUNCIL
REPORTS AND MEMORANDA

# The Calculation of the Pressure Distribution on Thick Wings of Small Aspect Ratio at Zero Lift in Subsonic Flow

*By*
J. WEBER, Dr.rer.nat.



LONDON: HER MAJESTY'S STATIONERY OFFICE
1957
THIRTEEN SHILLINGS NET

# The Calculation of the Pressure Distribution on Thick Wings of Small Aspect Ratio at Zero Lift in Subsonic Flow

By

J. WEBER, Dr.rer.nat.

COMMUNICATED BY THE PRINCIPAL DIRECTOR OF SCIENTIFIC RESEARCH (AIR),
MINISTRY OF SUPPLY

*Reports and Memoranda No.* 2993

*September*, 1954

*Summary.*—The method of expressing the velocity increment over aerofoils directly in terms of the section ordinates (Refs. 1 and 2) is extended to cover also straight and swept wings of finite aspect ratio. The wings considered are untapered in plan-form but may be tapered in thickness. The section can be of any given shape so that in this sense the analysis is more general than that of Refs. 3 to 6 which deal with wings of biconvex section.

The coefficients required in the calculation are tabulated for the centre-section of straight and swept-back wings ($\varphi = 0$ deg, $\varphi = 45$ deg and $\varphi = 60$ deg) of aspect ratios $0 \cdot 5$ ; 1 ; 2 ; and 4, the wing of infinite aspect ratio having been treated in Ref. 1. The remaining calculations can be made very quickly.

Since wings of very small aspect ratio can be treated also by the method of slender-body theory, the relations between linear theory, slender-body theory, and linearised slender-body theory are discussed. For the special case of ellipsoids, the results obtained from the various methods are compared with the exact solution.

1. *Introduction.*—Up to now the pressure distribution at zero lift on wings of any given symmetrical section shape has been calculated only for straight and sheared wings of infinite aspect ratio and for the centre-section of swept wings of infinite aspect ratio (*see, e.g.*, Refs. 1 and 2).

On wings of finite aspect ratio the pressure distribution may differ from the distribution on the corresponding two-dimensional wing for several reasons. This can clearly be seen if the wing is replaced by equivalent source-sink distributions. With a wing of finite aspect ratio, the source lines are cut off at the wing tips. This affects the velocity component normal to the chordal plane as well as the velocity increment in the direction of the main stream.

Further three-dimensional effects are produced by a tapered plan-form and by a spanwise variation of the section shape. A tapered plan-form results in a pattern of source-sink lines of varying sweep while changes in section shape (*e.g.*, varying thickness/chord ratio) alter the local strength of the source-sink distribution and hence the induced velocity.

So far, no attempt has been made to take all these effects fully into account. Approximate solutions can be obtained, if the simplifying assumptions of linearised theory or of slender-body theory or of both together are made. This report deals with these three methods.

In the linear theory, it is assumed that the wing thickness is small compared with the chord and the span. The effect of finite aspect ratio on the normal velocity component is ignored and

R.A.E. Report Aero. 2519, received 14th March, 1955.

the streamwise velocity component $v_x$ is calculated in the chordal plane instead of on the wing surface. With these simplifications, the work reduces to finding $v_x(x,y,0)$ from the known source distribution $q(x,y)$ by evaluating a double integral over the whole wing area.

This integral can be determined explicitly for wings with biconvex or other related sections in some simple cases, or otherwise numerically. Neumark and Collingbourne[3,4] (1949 and 1951) have given solutions for wings of finite aspect ratio, that are tapered in plan-form but not in thickness/chord ratio; and Newby[5] (1955) has considered in detail the practically important case of thickness taper; a simple case has also been treated in Ref. 7 (1950). Although Newby has succeeded in establishing the general trends produced by the various parameters, the actual results which he has obtained for the biconvex section cannot be applied with certainty to conventional aerofoil sections. Anyway, pressure distributions can never be worked out in advance since there are too many parameters involved, not only concerning the section shape but also the plan-form of the wing. Newby has dealt with this dilemma by approximating results obtained for the biconvex section, say, by factors applied to the standard distributions for the infinite sheared wing or centre distributions, the factors depending on thickness taper, plan-form taper, and sweep; it is then assumed that the same factors can be retained for wings with any given section shape where the two standard distributions can easily be obtained.

Here, another approach to the problem is attempted, applicable *ab initio* for sections of any shape, whereby the main body of the numerical calculation is done in advance once and for all, leaving a routine method which can easily be performed. This is possible for those plan-forms and spanwise variations of the thickness distribution in which the spanwise integration of the double integrals mentioned above can be performed explicitly, by using for the chordwise integration the method of mechanical quadrature by Gauss. This method has been applied in Ref. 1 to two-dimensional aerofoils, and it will be shown below that a similar treatment is possible for wings of finite aspect ratio. In this method the velocity increment is expressed as the sum of products of the section ordinates at fixed chordwise positions and certain coefficients, which are determined by the geometry of the wing but are independent of the section shape. It is thus possible to deal with wings of any section shape quite easily. These coefficients can be worked out in advance. A routine calculation method is thus developed, which is very quick; and the actual computing work is of the same order for the finite aspect ratio wing as for the two-dimensional wing.

The coefficients can be worked out for wings of any given aspect ratio with linear plan-form and thickness taper. However, the numerical calculation of the coefficients is rather lengthy. Therefore, numerical values of the coefficients have been given only for three simple cases:

(i) The centre-section of rectangular wings of constant section shape

(ii) the centre-section of rectangular wings for which the thickness-chord ratio is varying linearly along the span

(iii) the centre-section of untapered swept wings, $\varphi = 45$ deg and 60 deg, of constant section shape.

The coefficients are given for wings of aspect ratio $0 \cdot 5$ and greater, since for smaller values of the aspect ratio the simpler method of linearised slender-body theory may be applied. The determination of the coefficients is described in sections 2, 3 and 4.

The assumptions made in linear theory and their effects on the velocity distribution are discussed in section 5. Here a simple way to obtain a better approximation near the leading edge is suggested.

For the three cases, in which the coefficients have been calculated numerically, the effect of section shape is shown in section 6 by comparing the calculated velocity distributions on wings with a conventional section shape (RAE 101) and with biconvex section. This comparison is made to illustrate how far the results for wings with biconvex section give the general trends due to the various parameters and how much the actual values for a conventional section shape may differ from those for a biconvex section.

The application of the results obtained by linear theory to sub-critical compressible flow is briefly discussed in section 7. Supersonic flow is not treated at all.

For wings of very small aspect ratio, it is possible to justify the assumptions of slender-body theory, namely, that wing thickness and span are small compared with the wing chord. The application of slender-body theory for the determination of the thickness effect on small aspect ratio wings, as given, *e.g.*, by Adams and Sears[8] (1953), is discussed in section 8. The work is reduced to the determination, for each transverse plane, of a two-dimensional velocity potential which has a given derivative normal to the boundary of the cross-section. A method is given for determining this potential, if the cross-section is bounded by a simply connected curve, *i.e.*, if the trailing edge is straight or swept forward. The determination of the required conformal transformation of the cross-section into a circle is not discussed here. Finally the combination of linear theory and slender-body theory, as suggested by Keune[9] (1952), is discussed.

In the last section the velocities on ellipsoids with three different axes are calculated by the various approximate methods and compared with the exact solution.

2. *Rectangular Wings of Constant Section Shape.*—In this section the simplest case, namely rectangular wings with the same section along the whole span, is treated.

A rectangular co-ordinate system $x$, $y$, $z$ with the $x$-axis along the main stream and $y$ in the spanwise direction is used. The origin, $x = 0$, $y = 0$, $z = 0$ is at the leading edge of the centre-section. All dimensions are referred to the wing chord $c$, which is taken as unity. The semi-span of the wing is $s$.

A straight wing of constant chord and the same symmetrical section shape $z(x)$ along the whole span in a uniform flow of velocity $V_0$ at zero lift can be represented by a distribution of source and sink lines, $-s \leqslant y \leqslant s$, in the chordal plane; the strength $q(x)$ of the source lines according to linear theory is

$$q(x) = 2V_0 \frac{dz(x)}{dx} \quad \ldots \quad (1)$$

This source distribution produces at a point ($x$, $y$, $z = 0$) in the chordal plane a velocity component $v_x$ in the direction of the main stream:

$$v_x(x,y,0) = \int_0^1 dx' \int_{-s}^{+s} \frac{q(x')\,dy'}{4\pi} \frac{x - x'}{\{(x - x')^2 + (y - y')^2\}^{3/2}} \,. \quad \ldots \quad (2)$$

The integration with respect to $y$ can be done first, *i.e.*, the velocity $dv_x$ induced by a single source line is determined first.

$$dv_x(x,y) = \frac{q(x')}{4\pi} \frac{dx'}{x - x'} \left[\frac{s - y}{\{(x - x')^2 + (s - y)^2\}^{1/2}} + \frac{s + y}{\{(x - x')^2 + (s + y)^2\}^{1/2}}\right] \quad (3)$$

and therefore

$$\lim_{|x-x'| \to 0} dv_x\,(x,y) = \frac{q(x')}{2\pi} \frac{dx'}{x - x'} = \lim_{s \to \infty} dv_x\,(x,y) \,. \quad \ldots \quad (4)$$

This means that for pivotal points close to the source line the effect of the finite source line is the same as that of an infinitely long source line, as can be seen directly from Fig. 1.

The total velocity increment is by equations (1), (2) and (3):

$$\frac{v_x(x,y)}{V_0} = \frac{1}{\pi} \int_0^1 \frac{1}{2} \frac{dz}{dx'} \left[\frac{s - y}{\{(x - x')^2 + (s - y)^2\}^{1/2}} + \frac{s + y}{\{(x - x')^2 + (s + y)^2\}^{1/2}}\right] \frac{dx'}{x - x'} \,. \quad (5)$$

Since, when the aspect ratio is not too small, the difference between the velocity distributions on the finite wing and the infinite aspect ratio wing is small, we write the velocity on the finite aspect ratio wing as the sum of a two-dimensional solution and a correction term. In the two-dimensional case, the limit as $s \to \infty$, the integral of equation (5) can for fixed positions $x_\nu$ be determined as the sum of products of the known section ordinates and certain coefficients, which are independent of the section shape (*see* the Appendix and Ref. 1):

$$\frac{v_x(x_\nu, A = \infty)}{V_0} = \frac{1}{\pi}\int_0^1 \frac{dz}{dx'}\frac{dx'}{x_\nu - x'} = S^{(1)}(x_\nu) = \sum_{\mu=1}^{N-1} s^{(1)}_{\mu\nu} z_\mu \,. \qquad (6)$$

By equations (5) and (6) the velocity on the finite wing becomes:

$$\frac{v_x(x,y)}{V_0} = S^{(1)}(x) - \frac{1}{\pi}\int_0^1 \frac{1}{2}\frac{dz}{dx'}\left[\frac{\{(x-x')^2+(s-y)^2\}^{1/2}-(s-y)}{\{(x-x')^2+(s-y)^2\}^{1/2}} + \frac{\{(x-x')^2+(s+y)^2\}^{1/2}-(s+y)}{\{(x-x')^2+(s+y)^2\}^{1/2}}\right]\frac{dx'}{x-x'} \,. \qquad (7)$$

The integrals in equations (5) and (7) are of the type:

$$J = \frac{1}{\pi}\int_0^1 \frac{dz}{dx'}\frac{f(x,x')\,dx'}{x-x'} \,. \qquad (8)$$

This is similar to that for the velocity increment of the two-dimensional wing, equation (6), when the source strength $q(x') = 2V_0(dz/dx')$ is replaced by $2V_0(dz/dx')f(x,x')$. The corresponding section shape is however varying with the pivotal point $x$. It is therefore not advisable to apply equation (6) directly, since it would involve the working out of a series of new section shapes. But, as shown in the Appendix, integrals of the type of equation (8) can for fixed points $x = x_\nu$ also be approximated by sums of products of the section ordinates $z_\mu = z(x_\mu)$ and new fixed coefficients which are independent of $z(x)$:

$$\frac{1}{\pi}\int_0^1 \frac{dz}{dx'}\frac{f(x,x')\,dx'}{x_\nu - x'} = \sum_{\mu=1}^{N-1} s^{(1)}_{\mu\nu}\left[f(x_\nu,x_\mu) + (x_\nu - x_\mu)\left(\frac{df(x_\nu,x')}{dx'}\right)_{x_\mu}\right] z_\mu \,. \qquad (9)$$

The necessary conditions are that the function $f(x,x')$ and its derivative $df(x,x')/dx'$ must be finite and continuous in the whole interval $0 \leqslant x' \leqslant 1$.

The velocity increment at a point $(x = x_\nu, y)$ on a rectangular wing of constant section $z(x)$ can therefore be calculated from the formula:

$$\frac{v_x(x_\nu,y)}{V_0} = S^{(1)}(x_\nu) - \sum_{\mu=1}^{N-1} s^{(6)}_{\mu\nu} z_\mu \qquad (10)$$

where

$$\begin{aligned} s^{(6)}_{\mu\nu} &= s^{(1)}_{\mu\nu}\left[\frac{1}{2}\frac{\{(x_\nu-x_\mu)^2+(s-y)^2\}^{1/2}-(s-y)}{\{(x_\nu-x_\mu)^2+(s-y)^2\}^{1/2}} - \frac{1}{2}\frac{(x_\nu-x_\mu)^2(s-y)}{\{(x_\nu-x_\mu)^2+(s-y)^2\}^{3/2}}\right. \\ &\qquad \left. + \frac{1}{2}\frac{\{(x_\nu-x_\mu)^2+(s+y)^2\}^{1/2}-(s+y)}{\{(x_\nu-x_\mu)^2+(s+y)^2\}^{1/2}} - \frac{1}{2}\frac{(x_\nu-x_\mu)^2(s+y)}{\{(x_\nu-x_\mu)^2+(s+y)^2\}^{3/2}}\right] \\ &= s^{(1)}_{\mu\nu}\left[1 - \frac{(s-y)[2(x_\nu-x_\mu)^2+(s-y)^2]}{2\{(x_\nu-x_\mu)^2+(s-y)^2\}^{3/2}}\right. \\ &\qquad \left. - \frac{(s+y)[2(x_\nu-x_\mu)^2+(s+y)^2]}{2\{(x_\nu-x_\mu)^2+(s+y)^2\}^{3/2}}\right] \end{aligned} \qquad (11)$$

$$s^{(6)}_{\nu\nu} = 0 \,. \qquad (12)$$

Equation (12) is a consequence of the fact that the integrand in equation (7) vanishes for $x' = x$, as can be seen by writing equation (7) in the form:

$$\frac{v_x(x,y)}{V_0} = S^{(1)}(x) - \frac{1}{\pi}\int_0^1 \frac{1}{2}\frac{dz}{dx'}\left\{\frac{x - x'}{\{(x-x')^2 + (s-y)^2\}^{1/2}[\{(x-x')^2 + (s-y)^2\}^{1/2} + s - y]}\right.$$

$$\left. + \frac{x - x'}{\{(x-x')^2 + (s+y)^2\}^{1/2}[\{(x-x')^2 + (s+y)^2\}^{1/2} + s + y]}\right\} dx' . \qquad (13)$$

This agrees with equation (4) which states that in the neighbourhood of the source lines the finite source lines give the same contribution to the velocity increment as the infinitely long lines of the two-dimensional wing.

Equation (13) shows that the integrand vanishes for $x' = x$ even when the pivotal point $x$ coincides with the leading edge, since

$$\lim_{x \to 0} x \frac{dz}{dx} = 0$$

This means that equations (10) and (11) hold for $\nu = N$, i.e., $x_\nu = 0$, with $S^{(1)}(0)$ from equation (6–16) in Ref. 1 and

$$s_{\mu N}^{(1)} = \frac{(-1)^\mu - 1}{N} \frac{2 \sin \vartheta_\mu}{(1 + \cos \vartheta_\mu)^2} . \qquad (14)$$

Since

$$s_{\mu\nu}^{(1)} = 0 \qquad \text{for } \nu + \mu \text{ even}$$

$$s_{\mu\nu}^{(6)} = 0 \qquad \text{for } \nu + \mu \text{ even} . \qquad (15)$$

From

$$s_{\mu\nu}^{(1)} = s_{N-\mu,\, N-\nu}^{(1)}$$

and

$$(x_\nu - x_\mu)^2 = [(1 - x_{N-\nu}) - (1 - x_{N-\mu})]^2 = (x_{N-\nu} - x_{N-\mu})^2 \qquad (16)$$

it follows that

$$s_{\mu\nu}^{(6)} = s_{N-\mu,\, N-\nu}^{(6)} .$$

To determine the velocity increment on a finite wing by equations (10) and (11) is still tedious, but the coefficients $s_{\mu\nu}^{(6)}$ can be calculated in advance.

For the special case of the centre-section, $y = 0$,

$$s_{\mu\nu}^{(6)} = s_{\mu\nu}^{(1)} \left[1 - \frac{s[2(x_\nu - x_\mu)^2 + s^2]}{\{(x_\nu - x_\mu)^2 + s^2\}^{3/2}}\right] . \qquad (17)$$

The velocity increment can within linear theory be calculated from equation (10) to any desired degree of accuracy by taking in equation (9) a large number ($N$) of points along the chord. It has been shown in Ref. 1 that it is usually sufficient to take $N = 16$ when determining the basic term $S^{(1)}(x)$. The required value of $N$ for the term $\sum_{\mu=1}^{N-1} s_{\mu\nu}^{(6)} z_\mu$ can be found by evaluating the term for various $N$ or more easily for wings with biconvex section by comparing the result from equation (10) with the exact result obtained from equations (5) or (7) by explicit integration. Such a comparison is made in section 6; it shows that for spanwise stations that are more than half the wing chord away from the tips, or for the centre-section of wings with an aspect ratio greater than one, it is sufficient to take $N = 8$, *i.e.*, to approximate the section shape by an interpolation function which has the correct values at the leading edge and trailing edge and 7 points along the chord. This is advisable only for the correction term whilst the basic two-dimensional term $S^{(1)}(x)$ should be calculated with $N = 16$. This is the reason for expressing the velocity increment by two sums since thus a smaller number of coefficients $s_{\mu\nu}^{(6)}$ need to be worked out. The numerical values of the coefficients $s_{\mu\nu}^{(6)}$, from equation (17), for the centre section of wings of aspect ratio 4, 2, 1 and 0·5 are given in Table 1. Some calculated pressure distributions are plotted in Figs. 3 and 4 and are discussed in section 6. The calculations have been restricted to wings of aspect ratios greater than 0·5, since for wings with very small aspect ratio the method of linearised slender-body theory may be applied. The velocity on wings of small aspect ratio is of interest, when investigating the velocity on wings in subsonic compressible flow by means of the Prandtl-Glauert analogy. At sub-critical speeds wings with an aspect ratio of less than 0·5 are seldom of interest. A wing with aspect ratio 0·5 is analogous to a wing of aspect ratio 1·6 for a free-stream Mach number $M_0 = 0{\cdot}95$; or to a wing of aspect ratio 2·5 at $M_0 = 0{\cdot}98$. Moreover local supersonic regions must be expected below those Mach numbers in many practical cases, and this will invalidate the assumptions made in the theory, anyway.

3. *Rectangular Wings with Linearly Varying Thickness/Chord Ratio.*—This section deals with straight wings of constant chord with the same section shape along the span but with a thickness/chord ratio that is decreasing linearly from the centre-section to the tip. In linear theory, a wing given by

$$z(x,y) = z(x,0)(1 - \delta\,|y|)$$

is replaced by the source distribution:

$$\begin{aligned} q(x,y) &= q(x,y=0)(1 - \delta\,|y|) \\ &= 2V_0 \frac{dz(x,y=0)}{dx}(1 - \delta\,|y|) \qquad (18) \end{aligned}$$

Denoting by $t_c$ and $t_T$ the maximum thickness of the centre and tip sections,

$$\delta = \frac{t_c - t_T}{st_c} \,. \qquad (19)$$

To evaluate the streamwise velocity increment produced by this source distribution, we again determine the contribution of one source line first, *i.e.*, we perform the integration along $y$. The source line at $x'$, $-s \leqslant y' \leqslant s$, $z = 0$ produces at the point $x,y,z = 0$ the velocity component

$$\begin{aligned} dv_x(x,y) &= \int_{-s}^{0} \frac{q(x',0)\,dx'\,dy'}{4\pi}(1 + \delta y')\frac{x - x'}{\{(x - x')^2 + (y - y')^2\}^{3/2}} \\ &\quad + \int_0^s \frac{q(x',0)\,dx'\,dy'}{4\pi}(1 - \delta y')\frac{x - x'}{\{(x - x')^2 + (y - y')^2\}^{3/2}} \\ &= \frac{q(x',0)}{4\pi}\,\frac{dx'}{x - x'}\left\{\frac{s - y}{\{(x - x')^2 + (s - y)^2\}^{1/2}} + \frac{s + y}{\{(x - x')^2 + (s + y)^2\}^{1/2}}\right. \\ &\quad + \delta\left[\frac{(x - x')^2 - y(s - y)}{\{(x - x')^2 + (s - y)^2\}^{1/2}} + \frac{(x - x')^2 + y(s + y)}{\{(x - x')^2 + (s + y)^2\}^{1/2}}\right. \\ &\quad \left.\left. - 2\{(x - x')^2 + y^2\}^{1/2}\right]\right\}. \end{aligned}$$

For $y > 0$:

$$dv_x(x,y) = \frac{q(x',0)}{4\pi} \frac{dx'}{x - x'} \left\{(1 - \delta y) \left[\frac{s - y}{\{(x - x')^2 + (s - y)^2\}^{1/2}} + \frac{s + y}{\{(x - x')^2 + (s + y)^2\}^{1/2}}\right]\right.$$

$$+ \delta \left[\frac{(x - x')^2}{\{(x - x')^2 + (s - y)^2\}^{1/2}} + \frac{(x - x')^2}{\{(x - x')^2 + (s + y)^2\}^{1/2}}\right.$$

$$\left.\left. + 2y \frac{s + y}{\{(x - x')^2 + (s + y)^2\}^{1/2}} - 2\{(x - x')^2 + y^2\}^{1/2}\right]\right\} \quad \ldots \quad (20)$$

and

$$\lim_{|x' - x| \to 0} dv_x(x,y) = \frac{q(x',0)}{2\pi} (1 - \delta y) \frac{dx'}{x - x'}$$

$$= \frac{q(x',y)}{2\pi} \frac{dx'}{x - x'} \quad \ldots \quad (21)$$

which means that for a pivotal point near the source line the velocity increment is like that of an infinitely long source line of a strength that is constant along the span and equal to that at the local station considered.

Using equations (5), (10) and (20), the total velocity increment is:

$$\frac{v_x(x_\nu,y)}{V_0} = (1 - \delta y) \left[S^{(1)}(x_\nu) - \sum_{\mu=1}^{N-1} s^{(6)}_{\mu\nu} z_\mu\right]$$

$$- \delta \left\{\frac{1}{\pi}\int_0^1 \frac{dz}{dx'} \{(x_\nu - x')^2 + y^2\}^{1/2} \frac{dx'}{x_\nu - x'} - \frac{1}{\pi}\int_0^1 \frac{dz}{dx'} \frac{y(s + y)}{\{(x_\nu - x')^2 + (s + y)^2\}^{1/2}} \frac{dx'}{x_\nu - x'}\right.$$

$$\left. - \frac{1}{\pi}\int_0^1 \frac{1}{2} \frac{dz}{dx'} \left[\frac{(x_\nu - x')^2}{\{(x_\nu - x')^2 + (s - y)^2\}^{1/2}} + \frac{(x_\nu - x')^2}{\{(x_\nu - x')^2 + (s + y)^2\}^{1/2}}\right] \frac{dx'}{x_\nu - x'}\right\} . \quad (22)$$

The integrals are again of the type of equation (8), but the derivative $df(x,x')/dx'$ of the term $f(x,x') = \{(x - x')^2 + y^2\}^{1/2}$ in the first integral is discontinuous for $y = 0$ at the point $x' = x$, jumping from $-1$ to $+1$. This means that the approximation (9) must not be used for the integral

$$\lim_{y \to 0} \frac{1}{\pi}\int_0^1 \frac{dz}{dx'} \{(x_\nu - x')^2 + y^2\}^{1/2} \frac{dx'}{x_\nu - x'} .$$

Furthermore, for small values of $y$ the derivative is changing fairly rapidly in the neighbourhood of $x' = x$, which implies that an interpolation formula for $z(x') \dfrac{df(x,x')}{dx'}$ which takes into account only a few values along the chord (such as $N = 8$) need not give a good approximation. This is not a special feature of the present method, but will arise in all methods for numerical evaluation of the double integral, *e.g.*, in the method by F. Hjelte[6] (1952) which consists in 'dividing the wing area into a number of small subregions, performing the integration approximately in each of them, and adding the results.'

For $y \neq 0$, by equations (9) and (22):

$$\frac{v_x(x_\nu,y)}{V_0} = (1 - \delta y)\left[S^{(1)}(x_\nu) - \sum_{\mu=1}^{N-1} s^{(6)}_{\mu\nu} z_\mu\right] - \delta \sum_{\mu=1}^{N-1} s^{(7)}_{\mu\nu} z_\mu \qquad (23)$$

where

$$s^{(7)}_{\mu\nu} = s^{(1)}_{\mu\nu}\left[\{(x_\nu - x_\mu)^2 + y^2\}^{1/2} - \frac{(x_\nu - x_\mu)^2}{\{(x_\nu - x_\mu)^2 + y^2\}^{1/2}}\right.$$

$$- \frac{y(s+y)}{\{(x_\nu - x_\mu)^2 + (s+y)^2\}^{1/2}} - \frac{y(s+y)(x_\nu - x_\mu)^2}{\{(x_\nu - x_\mu)^2 + (s+y)^2\}^{3/2}}$$

$$- \frac{(x_\nu - x_\mu)^2}{2\{(x_\nu - x_\mu)^2 + (s-y)^2\}^{1/2}} - \frac{(x_\nu - x_\mu)^2}{2\{(x_\nu - x_\mu)^2 + (s+y)^2\}^{1/2}}$$

$$\left. + \frac{(x_\nu - x_\mu)^2[(x_\nu - x_\mu)^2 + 2(s-y)^2]}{2\{(x_\nu - x_\mu)^2 + (s-y)^2\}^{3/2}} + \frac{(x_\nu - x_\mu)^2[(x_\nu - x_\mu)^2 + 2(s+y)^2]}{2\{(x_\nu - x_\mu)^2 + (s+y)^2\}^{3/2}}\right]$$

$$= s^{(1)}_{\mu\nu}\left[\frac{y^2}{\{(x_\nu - x_\mu)^2 + y^2\}^{1/2}} - \frac{y(s+y)[2(x_\nu - x_\mu)^2 + (s+y)^2]}{\{(x_\nu - x_\mu)^2 + (s+y)^2\}^{3/2}}\right.$$

$$\left. + \frac{(x_\nu - x_\mu)^2(s-y)^2}{2\{(x_\nu - x_\mu)^2 + (s-y)^2\}^{3/2}} + \frac{(x_\nu - x_\mu)^2(s+y)^2}{2\{(x_\nu - x_\mu)^2 + (s+y)^2\}^{3/2}}\right] \qquad (24)$$

$$s^{(7)}_{\nu\nu} = 0$$

which follows from equation (21). Again the coefficients $s^{(7)}_{\mu\nu}$ can be worked out in advance.

In the numerical examples given in this report, only the most interesting station, the centre-section $y = 0$, has been considered, the coefficients for other sections have not yet been calculated.

At the centre-section, $y = 0$, by equation (22):

$$\frac{v_x(x_\nu,0)}{V_0} = S^{(1)}(x_\nu) - \sum_{\mu=1}^{N-1} s^{(6)}_{\mu\nu} z_\mu$$

$$- \delta\left[\frac{1}{\pi}\int_0^1 \frac{dz}{dx'}\{(x_\nu - x')^2\}^{1/2}\frac{dx'}{x_\nu - x'} - \frac{1}{\pi}\int_0^1 \frac{dz}{dx'}\frac{(x_\nu - x')^2}{\{(x_\nu - x')^2 + s^2\}^{1/2}}\frac{dx'}{x_\nu - x'}\right] \qquad (25)$$

As stated above, the approximation of equation (A–6) cannot be applied to the integral

$$\int_0^1 \frac{dz}{dx'}\{(x_\nu - x')^2\}^{1/2}\frac{dx'}{x_\nu - x'}$$

since $\dfrac{df(x,x')}{dx'}$ is discontinuous at $x' = x_\nu$. But it can be determined explicitly.

The result is

$$\int_0^1 \frac{dz}{dx'}\frac{\{(x_\nu - x')^2\}^{1/2}}{x_\nu - x'}\,dx' = \int_0^{x_\nu}\frac{dz}{dx'}\,dx' - \int_{x_\nu}^1 \frac{dz}{dx'}\,dx' = 2z(x_\nu,0) = -\frac{2}{\delta}\frac{\partial z(x,y)}{\partial|y|} \qquad (26)$$

since $z(x,y) = z(x,0)(1 - \delta|y|)$.

On the whole, the existence of a term $\dfrac{\Delta V}{V_0} = \dfrac{2}{\pi}\dfrac{\partial z(x,y)}{\partial|y|} = -\dfrac{2\delta}{\pi}z(x,0)$ which is proportional to the shape $z(x)$ itself, is an important feature introduced by the thickness taper. Without thickness taper, only two kinds of terms occurred in the expressions for the velocity increment: one being similar to that for two-dimensional aerofoils; and on swept wings a 'kink term' appears which is proportional to the local slope of the aerofoil (*see* equation (33) below). The kink term is caused by the sudden change in direction of the source lines, *i.e.*, by the change of the neighbouring source lines. The new term is caused by the sudden change in $\partial z/\partial y$.

The approximation of equation (A–6) is applicable to the second integral in equation (25), so that the velocity increment can be determined from the relation:

$$\frac{v_x(x_\nu,0)}{V_0} = S^{(1)}(x_\nu) - \sum_{\mu=1}^{N-1} s^{(6)}_{\mu\nu} z_\mu - \delta \left[\frac{2}{\pi} z(x_\nu) - \sum_{\mu=1}^{N-1} s^{(8)}_{\mu\nu} z_\mu \right] \quad \ldots \quad (27)$$

with $s^{(6)}_{\mu\nu}$ from equation (17) and

$$s^{(8)}_{\mu\nu} = - s^{(1)}_{\mu\nu} \frac{s^2(x_\nu - x_\mu)^2}{\{(x_\nu - x_\mu)^2 + s^2\}^{3/2}} . \quad \ldots \quad (28)$$

Again:

$$s^{(8)}_{\nu\nu} = 0 \quad \ldots \quad (29)$$

$$s^{(8)}_{\mu\nu} = 0 \text{ for } \nu + \mu \text{ even} \quad \ldots \quad (30)$$

$$s^{(8)}_{\mu\nu} = s^{(8)}_{N-\mu,\, N-\nu} \quad \ldots \quad (31)$$

$$\frac{v_x(x = 0, y = 0)}{V_0} = S^{(1)}(0) - \sum_{\mu=1}^{N-1} s^{(6)}_{\mu N}\, z_\mu + \delta \sum_{\mu=1}^{N-1} s^{(8)}_{\mu N}\, z_\mu . \quad \ldots \quad (32)$$

The coefficients $s^{(8)}_{\mu\nu}$ from equation (28) for $A = 4$, 2, 1, $N = 8$ and $A = 0 \cdot 5$, $N = 16$, are tabulated in Table 2, and calculated velocity distributions are given in Figs. 3 and 4.

4. *Untapered Swept Wings of Constant Section Shape.*—The effect of finite aspect ratio will depend on the angle of sweep of the wing. To determine this variation we calculate the velocity increment at the centre-section of swept wings with constant chord and constant section shape along the span.

Within linear theory, such wings can be represented by a distribution of kinked source lines, which are of constant strength along the line. It is known from the evaluation of the velocity distributions at the centre section of swept wings of infinite aspect ratio[2] that a kinked source line has a singular behaviour at the centre-section different from that of a straight line. This explains the occurrence of the 'kink term.'

The velocity increment on the infinite aspect ratio wing is (*see, e.g.*, Ref. 2):

$$\frac{v_{x\infty}(x,y = 0)}{V_0} = \cos\varphi \,.\, S^{(1)}(x) - \cos\varphi \,.\, f(\varphi) S^{(2)}(x) \quad \ldots \quad (33)$$

with

$$S^{(2)}(x) = \frac{dz}{dx} = \sum_{\mu=1}^{N-1} s^{(2)}_{\mu\nu} z_\mu . \quad \ldots \quad (34)$$

Since the kink term, $\cos\varphi \,.\, f(\varphi) S^{(2)}(x)$, is caused by the sudden change in the direction of the source lines in the immediate neighbourhood of the pivotal point, it will be the same for wings of both infinite and finite aspect ratio. To avoid reconsidering the complications arising from this singularity, the velocity increment on the wing of finite aspect ratio is calculated as the difference between the velocity distribution on the infinite wing and the contribution of the semi-infinite source lines outside the tips of the wing, which of course do not exist in the case of the finite wing.

Two semi-infinite source lines $s \leqslant |y'| < \infty$, swept by an angle $\varphi$, which when extended would pass through the point $x',y = 0$ produce at the point $x,y = 0$ the velocity increment:

$$dv_x = 2\int_s^\infty \frac{q(x')\,dx'\,dy'}{4\pi}\,\frac{x - x' - y'\tan\varphi}{\{(x - x' - y'\tan\varphi)^2 + y'^2\}^{3/2}}$$

$$= \frac{q(x')}{2\pi}\,\frac{dx'}{x - x'}\cos\varphi\,\frac{\{\cos^2\varphi\,.\,(x - x')^2 - \sin 2\varphi\,.\,(x - x')s + s^2\}^{1/2} - s}{\{\cos^2\varphi\,.\,(x - x')^2 - \sin 2\varphi\,.\,(x - x')s + s^2\}^{1/2}} \quad \ldots \quad (35)$$

Hence for the finite wing:

$$\frac{v_x(x,0)}{V_0} = \cos\varphi\,.\,S^{(1)}(x) - \cos\varphi\,.\,f(\varphi)S^{(2)}(x)$$

$$- \cos\varphi\,.\,\frac{1}{\pi}\int_0^1 \frac{dz}{dx'}\,\frac{\{\cos^2\varphi\,.\,(x - x')^2 - \sin 2\varphi\,.\,(x - x')s + s^2\}^{1/2} - s}{\{\cos^2\varphi\,.\,(x - x')^2 - \sin 2\varphi\,.\,(x - x')s + s^2\}^{1/2}}\,\frac{dx'}{x - x'} \quad (36)$$

$$\frac{v_x(x_\nu,0)}{V_0} = \cos\varphi\,.\,S^{(1)}(x_\nu) - \cos\varphi\,.\,f(\varphi)S^{(2)}(x_\nu) - \cos\varphi\sum_{\mu=1}^{N-1} s^{(6)}_{\mu\nu}z_\mu \quad \ldots \quad \ldots \quad \ldots \quad (37)$$

where

$$s^{(6)}_{\mu\nu} = s^{(1)}_{\mu\nu}\left\{1 - \frac{s[2\cos^2\varphi\,.\,(x_\nu - x_\mu)^2 - 1\cdot5\sin 2\varphi\,.\,(x_\nu - x_\mu)s + s^2]}{\{\cos^2\varphi\,.\,(x_\nu - x_\mu)^2 - \sin 2\varphi\,.\,(x_\nu - x_\mu)s + s^2\}^{3/2}}\right\} \quad \ldots \quad \ldots \quad (38)$$

$$s^{(6)}_{\nu\nu} = 0 \quad \ldots \quad (39)$$

$$s^{(6)}_{\mu\nu} = 0 \text{ for } \mu + \nu \text{ even} \quad \ldots \quad (40)$$

but $\quad s^{(6)}_{\mu\nu} \neq s^{(6)}_{N-\mu,\,N-\nu}$

since $x_\nu - x_\mu = -[x_{N-\nu} - x_{N-\mu}]$ .

Equation (39) is equivalent with the fact that the integrand in the integral of equation (36) vanishes for $x' = x$. This follows from the fact that for a pivotal point $(x,y = 0)$ near the kink of a source line $(x',y = 0)$ both the finite and the infinitely long source line give the same contribution to the velocity increment, which implies that the kink term does not vary with the aspect ratio. However the velocity distributions on the straight and the swept finite aspect ratio wing do not differ only by the 'kink term' since the contributions of the cut off source lines and therefore the coefficients $s^{(6)}_{\mu\nu}$ depend on the angle of sweep. Some numerical results are plotted in Figs. 5, 6 and 7 and are discussed in section 6.

The values $s^{(6)}_{\mu\nu}$ from equation (17) given in Table 1, are for the special case $\varphi = 0$. Values for $\varphi = 45$ deg and $\varphi = 60$ deg are tabulated in Tables 3 and 4.

The above formulae give only the velocity increments at the centre-section. For any spanwise station the formulae naturally become more complicated, as may be seen from the relation for the velocity at any spanwise station of a swept wing of infinite aspect ratio. It is:

$$\frac{v_x(x,y,0)}{V_0} = \cos\varphi\,.\,S^{(1)}(x)$$

$$- \frac{y\sin\varphi}{\pi}\int_0^1 \frac{dz}{dx'}$$

$$\frac{\{(x - x')^2\cos^2\varphi + (x - x')y\sin 2\varphi + y^2\}^{1/2} - y}{[(x - x') + 2y\tan\varphi]\{(x - x')^2\cos^2\varphi + (x - x')y\sin 2\varphi + y^2\}^{1/2}}\,\frac{dx'}{x - x'} \quad (41)$$

where $x$ is measured from the leading edge of the section considered. An approximation to the integral can again be obtained by a sum according to equation (A–6). For the interesting stations near the centre-section a check should be made as to whether it is sufficient to take $N = 8$. The coefficients in this case have not been calculated.

In the following analysis it will be shown that wings with tapered thickness or tapered plan-form lead to such complicated expressions that the coefficients for an arbitrary section shape have not been calculated.

To determine the velocity at the centre-section of a swept wing whose thickness/chord ratio is varying linearly along the span, one must not calculate the value at the chord of the centre-section but take the limit as $z \to 0$ of $v_x(x,0,z)$ or $\lim_{y \to 0} v_x(x,y,0)$, so as to obtain the correct centre term. This gives

$$\frac{v_x(x_\nu,0,0)}{V_0} = \lim_{z \to 0} \frac{1}{\pi} \int_0^1 \frac{dz}{dx'} dx' \int_0^s \frac{(1 - \delta y')(x_\nu - x' - y' \tan \varphi)}{\{(x_\nu - x' - y' \tan \varphi)^2 + y'^2 + z^2\}^{3/2}} dy'$$

$$= \cos \varphi \,.\, S^{(1)}(x_\nu) - \cos \varphi \,.\, f(\varphi) S^{(2)}(x_\nu)$$

$$- \cos \varphi \sum_{\mu=1}^{N-1} s_{\mu\nu}^{(6)} z_\mu - \delta \cos^2 \varphi \,.\, \frac{2}{\pi} z(x_\nu)$$

$$+ \delta \cos \varphi \,.\, \frac{1}{\pi} \int_0^1 \frac{dz}{dx'} \frac{\cos^2 \varphi \,.\, (x_\nu - x')^2 - s \sin 2\varphi \,.\, (x_\nu - x')}{\{\cos^2 \varphi \,.\, (x_\nu - x')^2 - s \sin 2\varphi \,.\, (x_\nu - x') + s^2\}^{1/2}} \frac{dx'}{x_\nu - x'}$$

$$+ \delta \sin \varphi \cos \varphi \frac{1}{\pi} \int_0^1 \frac{dz}{dx'} \times$$

$$\times \ln \left[ \frac{\{\cos^2 \varphi \, (x_\nu - x')^2 - s \sin 2\varphi \, (x_\nu - x') + s^2\}^{1/2} + s}{\cos \varphi} - \sin \varphi (x_\nu - x') \right] dx'$$

$$- \delta \sin \varphi \cos \varphi \frac{1}{\pi} \int_0^1 \frac{dz}{dx'} \ln \left[\{(x_\nu - x')^2 + z_\nu^2\}^{1/2} - \sin \varphi \,.\, (x_\nu - x')\right] dx' \,. \qquad .. \quad (42)$$

The approximation of equation (A–6) can be used to deal with the first and second integrals but not the third integral. A numerical calculation does not seem advisable in view of the complicated expressions contained in equation (42). This is not a special feature of the present method however, but is due to the type of source distribution.

The same type of integrals occur in the expression for the velocity distribution at the centre-section of a tapered wing of constant thickness/chord ratio, since

$$\frac{v_x(x_\nu,0,0)}{V_0} = \lim_{z \to 0} \frac{1}{\pi} \int_0^1 \frac{dz}{dx'} dx' \int_0^s \frac{(1 - \delta y')[x_\nu - x' - y'(\tan \varphi_{\mathrm{LE}} - \delta x')]}{\{[x_\nu - x' - y'(\tan \varphi_{\mathrm{LE}} - \delta x')]^2 + y'^2 + z^2\}^{3/2}} dy' \,. \qquad .. \quad (43)$$

One can therefore draw the conclusion that the determination of the velocity increments at any spanwise station of a swept tapered wing of a given thickness distribution is not a problem that is best solved by the usual numerical methods. It seems more suitable to be treated by an electric analogue computor.

5. *Discussion and Improvement of Linear Theory.*—Within linear theory three assumptions are made:

(i) The velocity increment $v_x$ is small compared with $V_0$

(ii) The velocity component $v_z(x,y,z)$ which is produced at the surface (by a source-sink distribution in the chordal plane) can be approximated by the velocity $v_z(x,y,0)$ produced at the chordal plane

(iii) The total velocity at the surface $V(x,y,z)$ can be approximated by the streamwise velocity $V_0 + v_x(x,y,0)$ at the chordal plane, neglecting the components $v_y$ and $v_z$.

There are three main cases where these assumptions are not satisfied and where it is to be expected that linear theory may not give satisfactory results:

(*a*) The region of the leading edge for conventional round-nosed sections on all aerofoils, whether the span is infinite or not

(*b*) The tip regions of wings of any finite aspect ratio

(*c*) The whole wing if the aspect ratio is small.

It will be shown that a correction to linearised theory can be found to obtain a solution in case (*a*). In case (*b*) an empirical correction has been determined (*see* Refs. 2 and 10). A special case of (*c*) is the group of wings of very small aspect ratio, which can be dealt with by slender-body theory. We will discuss the relation between linear theory and slender-body theory in section 8. In section 9 the case of ellipsoids will be used to show how accurately the velocity on small aspect ratio wings may be calculated by linear theory by comparison with the exact results.

We will discuss first some effects of the simplifications made in linear theory. Imagine a source distribution of strength $q(x,y)$ in the plane $z = 0$. At points away from the edges, the velocity component normal to the plane is equal to $\pm \frac{1}{2}q(x,y)$, since the source material is flowing out normal to the plane. Half of it emerges from the upper surface and the other half from the lower surface. For points at a small distance above or below the wing $v_z$ is approximately equal to $q/2$. At the edges of the source distribution, *i.e.*, at the leading and trailing edge and the tips, the source material can escape in all directions, *e.g.*, it can escape sideways near the tips. $v_z$ is then smaller than $\pm q(x)/2$ on the wing surface.

A distribution of finite source lines of constant spanwise strength thus produces near the ends of the source lines a smaller $v_z$ velocity than infinitely long lines and a non-zero $v_y$ velocity. This means that the wing represented by such source lines is thinner at the tips than at the centre but wider than the source lines. The source distribution used to represent a finite wing must be changed with the aspect ratio and must vary along the span; strictly it cannot be taken as that for a two-dimensional wing as is done in linear theory. Source distributions to represent square-cut wings* need to be stronger near the tips but are cut short†. It is likely that these two modifications have a small combined effect at sections away from the tips since the separate effects are of opposite sign. For wings of small aspect ratio, the fact that in linear theory the sources are spread over too wide a spanwise area will generally reduce the calculated streamwise velocity increment.

---

* Strictly square-cut wings cannot be represented by source distributions in the chordal plane alone. But one can obtain tip shapes which are a better approximation to square-cut tips than those resulting from constant spanwise source distributions.

† A similar difference between the exact source distribution and the one from linear theory exists near the leading edge of round-nosed two-dimensional wings. This difference may be illustrated on wings with elliptical section:

$$z(x) = \tfrac{1}{2}t\{1 - (1 - 2x)^2\}^{1/2}.$$

The exact source distribution obtained by the method of conformal transformation is:

$$\frac{q(x)}{2V_0} = \frac{t}{1 - t}\,\frac{1 - 2x}{\{1 - (t)^2 - (1 - 2x)^2\}^{1/2}}$$

$$\text{for } \frac{1 - \{1 - (t)^2\}^{1/2}}{2} < x < \frac{1 + \{1 - (t)^2\}^{1/2}}{2}.$$

From linear theory:

$$\frac{q(x)}{2V_0} = \frac{t\,(1 - 2x)}{\{1 - (1 - 2x)^2\}^{1/2}} \text{ for } 0 < x < 1.$$

The correct source distribution is stronger but has a shorter chordwise extent than the one from linear theory. The comparison must not be carried too far, since there is one important difference between the tips and the leading edge where assumption (i) does not hold.

There is, however, the further simplification implied in assumption (iii). Replacing the velocity increment $v_x(x,y,z)$ at the surface by $v_x(x,y,0)$ in the chordal plane has at least over part of the wing an effect of the opposite sign. For the maximum thickness position, $x_{\max}$,

$$|v_x(x_{\max},y,0)| \geqslant |v_x(x_{\max},y,z)|$$

as can be seen from the relation

$$v_x(x,y,z) = \iint\limits_{\substack{\text{wing}\\ \text{area}}} \frac{q(x',y')}{4\pi} \frac{x - x'}{\{(x - x')^2 + (y - y')^2 + z^2\}^{3/2}} \, dx' \, dy' \, . \qquad \qquad (44)$$

For a rectangular wing, the integration along $y$ can be done explicitly. We obtain instead of equation (5) for $y = 0$:

$$v_x(x,0,z) = \frac{1}{\pi} \int_0^1 \frac{dz}{dx'} \frac{s}{\{(x - x')^2 + s^2 + z^2\}^{1/2}} \frac{x - x'}{(x - x')^2 + z^2} \, dx' \, . \qquad \qquad (45)$$

As an example the velocities at the maximum thickness position, $x_{\max}$, of a 10 per cent thick rectangular wing with RAE 101 section have been calculated in the chordal plane and at the surface using in both cases the source distribution from linear theory:

| $A$ | $\frac{v_x}{V_0}(x_{\max}, y = 0, z = 0)$ | $\frac{v_x}{V_0}(x_{\max}, y = 0, z = t/2)$ |
|---|---|---|
| 0·1 | 0·048 | 0·029 |
| 1·0 | 0·131 | 0·104 |
| $\infty$ | 0·145 | 0·118 |

The difference in the $v_x$-values is appreciable. Since it is known that $v_x(z = 0)$ is a good approximation for the two-dimensional wing (*see* Ref. 1), the results show in particular that one does not obtain a satisfactory approximation for the velocity on the two-dimensional wing by calculating the $v_x$-velocity which the source distribution of the linear theory produces at the surface of the wing. This will mean that in general one does not improve the results of linear theory by calculating only the streamwise velocity increment at the surface. If a better approximation is needed, the $v_y$- and $v_z$-velocities must also be determined at the surface, which implies that a source distribution different from that of linear theory has to be taken.

That the effects of the various simplifications of linear theory cancel each other to a great extent for points away from the leading edge has been shown for two-dimensional wings in Ref. 1 and is shown for wings of small aspect ratio on a special example in section 9. We must however apply a correction to the results from linear theory near the leading edge.

It has been shown (*see, e.g.*, Ref. 1) that one obtains a very good approximation to the velocity along the whole surface of two-dimensional wings by multiplying the result from linear theory by the factor $\dfrac{1}{\{1 + (dz/dx)^2\}^{1/2}}$:

$$V(x,z) = \frac{V_x(x,0)}{\{1 + (dz/dx)^2\}^{1/2}}$$

$$= \frac{V_0 + v_x(x,0)}{\{1 + [S^{(2)}(x)]^2\}^{1/2}} \, . \qquad \qquad (46)$$

For aerofoils of elliptical cross-section equation (46) gives the exact velocity distribution; in this case

$$V(x,z) = \frac{V(x = 0 \cdot 5, z = t/2)}{\{1 + (dz/dx)^2\}^{1/2}} = \frac{V_{\max}}{\{1 + (dz/dx)^2\}^{1/2}} \, . \qquad \qquad (47)$$

The same relation is true for ellipsoids, both for axially symmetrical ones and for those having three different axes (*see* equation (102) in section 9):

$$V(x,y = 0,z) = \frac{V(x = 0 \cdot 5,\ y = 0,\ t/2)}{\{1 + (dz/dx)^2\}^{1/2}} . \quad \ldots \quad (48)$$

As shown in section 9, the values of $v_x(x,0,0)$ calculated by slender-body theory and linearised slender-body theory are constant along the chord of an ellipsoid, as is $v_x(x,z = 0)$ for the two-dimensional elliptic wing. The values $v_x(0 \cdot 5,\ 0,\ 0)$ from linear theory and linearised slender-body theory do, however, differ from the exact $v_x(0 \cdot 5,\ 0,\ t/2)$ by a term of the order $(t/c)^2$, whilst they are equal for the two-dimensional wing.

In view of these relations and the fact that close to the leading edge, except near the wing tips, the flow on a finite wing can be expected to be similar to that on a two-dimensional wing, we propose to apply the same factor to the results of linear theory, *i.e.*, to use equation (46) with the velocity increments $v_x(x,y,0)$ of the previous sections.

The effect of this correction is illustrated by Fig. 8, in which the velocities resulting from linear theory and those corrected by applying equation (46) are plotted together. It is shown, *e.g.*, that in some cases linear theory may give wrong values of the maximum velocity.

The following may be noted as a matter of interest. Wings with the conventional rounded tips but otherwise constant spanwise thickness may be represented—at least for calculating the velocity distribution at stations away from the tips—by a distribution of source lines of constant spanwise strength and two lines of three-dimensional sources at the beginning of the tips. The strength of the sources is according to the linear theory of bodies of revolution:

$$Q(x) = \tfrac{1}{2} \frac{d\pi z^2(x)}{dx} V_0 . \quad \ldots \quad (49)$$

By this method the two limiting cases of wings of infinite aspect ratio and the body of revolution are properly represented. The source distribution of equation (49) produces a velocity increment

$$\frac{\Delta v_x(x,y,z)}{V_0} = \tfrac{1}{4} \int_0^1 z(x') \frac{dz}{dx'} \frac{x - x' - \tan\varphi \, . \, (s - y)}{\{[x - x' - \tan\varphi \, . \, (s - y)]^2 + (s - y)^2 + z^2(x)\}^{3/2}} dx' . \quad \ldots \quad (50)$$

For a straight wing of aspect ratio $0 \cdot 5$ with elliptic section of 10 per cent thickness/chord ratio, the velocity increment at the mid-point ($x = 0 \cdot 5, y = 0, z = 0$) due to the three-dimensional sources is $\Delta v_x/V_0 = 0 \cdot 0054$. Equations (10) and (17) give the velocity increment

$$v_x(0 \cdot 5,\ 0,\ 0)/V_0 = 0 \cdot 1 - 0 \cdot 0354 = 0 \cdot 0646,$$

where $0 \cdot 1$ is the velocity increment of the two-dimensional wing. So that for the wing with rounded tips $v_x(0 \cdot 5,\ 0,\ 0)/V_0 = 0 \cdot 070$. The same numerical value is obtained by equations (10) and (17) for a rectangular wing of aspect ratio $0 \cdot 58$, *i.e.*, for a wing which has the same plan view area as the wing with rounded tips. This means that when calculating the pressure distribution due to thickness it is advisable to take a mean span and not the span at the trailing edge as is done when calculating the lift distribution.

6. *Numerical Results.*—In this section some numerical results are discussed. First, the accuracy obtained by approximating the integrals by finite sums is shown. For the biconvex section shape, the velocity increments on the straight untapered wing of finite aspect ratio

$A = 2s/c$, resulting from linear theory, *i.e.*, from equation (5), can be determined explicitly. The result is given in Ref. 3. These values are compared in the table below with the approximate results from equation (10) for the mid-chord point of the centre section, $x = 0 \cdot 5$, $y = 0$.

| $A$ | $\dfrac{v_x/V_0}{(v_x/V_0)_{A=\infty}}$ exact | $\dfrac{v_x/V_0}{(v_x/V_0)_{A=\infty}}$ equation (16) with $N =$ | |
|---|---|---|---|
| $\infty$ | 1·000 | | 1·000 |
| 4 | 0·990 | 8 | 0·990 |
| 2 | 0·962 | 8 | 0·963 |
| 1 | 0·881 | 8 | 0·885 |
| 0·5 | 0·721 | 8 | 0·819 |
| | | 16 | 0·724 |

This comparison shows that for $A \geqslant 1$ sufficiently accurate results are obtained with $N = 8$.

To illustrate the effect of the section shape, velocity distributions at the centre-section have been calculated for various wings with 10 per cent thick RAE 101 and biconvex sections. Equation (46) has been applied to the results from linear theory, as explained in the preceding section.

Figs. 3 and 4 give the velocity distribution at the lines of symmetry on unswept wings of constant chord, (*a*) with constant section shape along the span ($\delta = 0$) and (*b*) with a thickness/chord ratio decreasing linearly from $0 \cdot 1$ at the centre to zero at the tip ($\delta = 2/A$). The velocities on the finite wing are in general smaller than on the two-dimensional wing. The reduction of the maximum velocity is plotted in Fig. 9, it is nearly the same for the two section shapes. We can conclude from these numerical results that one obtains a fair approximation to the maximum velocity increment on a conventional section shape by reducing the two-dimensional value by a reduction factor obtained from the wing with biconvex section (*see* Ref. 5).

With three-dimensional wings of biconvex section the velocity distributions have nearly the same shape as on the two-dimensional wing. With a conventional section shape this is still nearly true for finite wings of constant thickness/chord ratio, but it is less true for wings with decreasing thickness. This implies that for the biconvex section a good approximation to the velocity at any chordwise position can be obtained by reducing the two-dimensional velocity by a constant reduction factor, *e.g.*, the one determined at the maximum thickness position. For the conventional section shape, this procedure still gives a reasonable value for the effect of finite aspect ratio, but it cannot be used to account for the effect of taper in thickness on the velocities over the front part of the wing.

The figures show that the same rate of decrease of the maximum thickness $\partial z(x,y)/\partial y = -\delta z(x,0)$, brings a greater reduction in the velocity increment on the larger aspect ratio wing. Crudely, the same reduction is obtained if the product $\delta . A$ is the same.

Velocity distributions at the centre-section of swept wings of constant chord and constant spanwise thickness distribution have been calculated for aspect ratios $0 \cdot 5$, $1 \cdot 0$ and $2 \cdot 0$. The velocity distributions for wings of aspect ratios 1 and 2 lie very close to those for the infinite wings and are therefore not plotted, the maximum velocities are given in Fig. 9. We thus obtain the result that for wings of aspect ratio greater than one the effect of the finite aspect ratio is small. This fact was also found by experiments on 53-deg swept wings (*see* Refs. 2 and 11), where within the accuracy of the tests, the same pressure distribution was measured at the centre-sections of two wings of aspect ratio $1 \cdot 05$ and $2 \cdot 0$.

The velocity distributions on wings of aspect ratio 0·5 are plotted in Figs. 5 and 6 together with the distributions on infinite wings. In these calculations, equation (46) has again been applied to the results from linear theory, equation (37). Fig. 5 shows that for the RAE 101 section the maximum velocity is about the same for the finite aspect ratio wing and the infinite wing.

To illustrate how the aspect ratio effect changes with the angle of sweep, the difference between the velocities on the infinite wings and the finite aspect ratio wings—as resulting from linear theory—is plotted in Fig. 7 for various angles of sweep. Whilst on the straight wing, the velocity decreases with decreasing aspect ratio for all points along the chord, there is on swept wings a considerable portion of the front part of the wing over which the velocity increases. This implies that the shape of the velocity distribution alters with aspect ratio, in particular the position of the maximum velocity is generally farther forward on the wing with small aspect ratio than on the infinite wing. We do not, therefore, obtain a good approximation to the velocity distribution on the finite swept wing by applying the procedure suggested for the straight wing, *i.e.*, by reducing the velocity on the infinite wing by a constant factor, as was suggested in Ref. 2. It will be preferable in many practical cases to make use of the refinement offered by the present method rather than to employ the less accurate method of Ref. 2. In those cases where the numerical values of the coefficients have been worked out, the velocity distribution can be calculated in about an hour, if the section co-ordinates at the fixed points $x_\nu$ are known.

7. *Application to Subcritical Compressible Flow.*—The method of the present report can be extended to be applicable to subcritical compressible flow by means of the usual flow analogy. In order to be consistent with the assumptions of linearised theory, the Prandtl-Glauert analogy in the form proposed by Göthert[12] (1941) should be applied. This states that the velocity increment $v_x$ in compressible flow is $1/\beta^2$ times the velocity increment $v_{xa}$ in incompressible flow on an analogous wing, obtained by reducing the lateral dimensions of the original wing in the ratio $\beta$ : 1. Here

$$\beta = (1 - M_0^2)^{1/2} \quad \ldots \quad (51)$$

and $M_0$ is the free-stream Mach number. From this, we obtain the well-known result that the velocity on a wing of finite aspect ratio rises less steeply with Mach number than on the corresponding two-dimensional aerofoil. This was first shown by Ludwieg[13] (1946). For unswept wings this is a consequence of the fact that, as the Mach number increases, the aspect ratio of the analogous wing decreases and with it the velocity increment. The effect of the aspect ratio is less on swept wings, as is demonstrated by the examples shown in Fig. 9, but the angle of sweep of the analogous wing increases with increasing Mach number, which results generally in a decreased velocity. The differences in the velocity distributions on finite swept wings of different section shape as shown in Figs. 5 and 6, imply that one cannot always draw generally valid conclusions about the effect of compressibility by using the results obtained for wings with biconvex section.

A further example of the velocity variation with Mach number can easily be obtained for the special case of rectangular wings with elliptic aerofoil sections of constant thickness/chord ratio along the span. By the Prandtl-Glauert analogy, the velocity increment in compressible flow is

$$\frac{v_x(x,y,z)}{V_0} = \frac{1}{4\pi\beta^2 V_0}\int_0^1\int_{-\beta s}^{\beta s} q_a(x')\,\frac{x - x'}{\{(x - x')^2 + \beta^2(y - y')^2 + \beta^2 z^2\}^{3/2}}\,dx'\,dy' \quad \ldots \quad (52)$$

where $q_a = 2V_0\beta \,.\, dz/dx$ is the source distribution representing the analogous wing. For a wing of elliptic section shape

$$z(x) = \tfrac{1}{2}t\{1 - (1 - 2x)^2\}^{1/2} \quad \ldots \quad (53)$$

$$q_a(x') = 2V_0\beta t\,\frac{1 - 2x'}{\{1 - (1 - 2x')^2\}^{1/2}} \quad \ldots \quad (54)$$

We calculate only the maximum velocity increment at $x = 0{\cdot}5$ on the centre line, $y = 0$, of the wing in the chordal plane, as in linear theory. Hence,

$$\frac{v_x(0{\cdot}5,0,0)}{V_0} = \frac{4}{\pi} ts \int_0^1 \frac{1}{\{1 - (1 - 2x')^2\}^{1/2}} \frac{1}{\{(1 - 2x')^2 + 4\beta^2 s^2\}^{1/2}} dx'$$

or, with the transformation $1 - 2x' = \cos\vartheta$,

$$\frac{v_x}{V_0} = \frac{4}{\pi} ts \int_0^{\pi/2} \frac{d\vartheta}{\{\cos^2\vartheta + 4\beta^2 s^2\}^{1/2}}$$

$$= \frac{4}{\pi} \frac{ts}{\{1 + 4\beta^2 s^2\}^{1/2}} \int_0^{\pi/2} \frac{d\vartheta}{\left\{1 - \frac{1}{1 + 4\beta^2 s^2} \sin^2\vartheta\right\}^{1/2}}$$

which leads to the complete elliptic integral of the first kind:

$$\frac{v_x}{V_0} = \frac{4}{\pi} \frac{ts}{\{1 + 4\beta^2 s^2\}^{1/2}} \mathbf{K}(k^2)$$

$$= \frac{2}{\pi} \frac{tA}{\{1 + \beta^2 A^2\}^{1/2}} \mathbf{K}(k^2) \text{ with } k^2 = \frac{1}{1 + \beta^2 A^2} \quad \ldots \quad (55)$$

This relation is plotted in Figs. 10 and 11. The velocity decrease with aspect ratio down to $A = 0{\cdot}5$ is about the same for the elliptic, biconvex and RAE 101 section, but the relative reduction is greatest for the elliptic section. Therefore, wings with elliptic section show the smallest velocity rise with Mach number compared with the two-dimensional aerofoil.

Assuming that either the aspect ratio of the wing is small ($A \ll 1$) or that the free-stream Mach number is near unity ($\beta \ll 1$), so that the analogous wing is of small aspect ratio, we obtain from equation (55)

$$\frac{v_x}{V_0} = \frac{2}{\pi} tA \ln \frac{4}{\beta A} + \ldots \quad \ldots \quad (56)$$

using the well-known expansion of $\mathbf{K}$ for $1 - k^2 \ll 1$, where the next term is of the order $\beta^2 A^2 \ln (1/\beta A)$.

Equation (56) corresponds to the relation derived from slender-body theory (*see* the next section):

$$\frac{v_x(x)}{V_0} = \left(\frac{v_x(x)}{V_0}\right)_{M_0=0} - \frac{1}{2\pi} S''(x) \ln \frac{1}{\beta} \quad \ldots \quad (57)$$

where $S''(x)$ is the second derivative of the cross-sectional area of the wing or body.

Relation (56) is compared in Fig. 10 with equation (55) for wings of 10 per cent thickness. The agreement up to aspect ratios of about 2 means that for rectangular wings of aspect ratio smaller than 2 the velocity increases with Mach number according to the logarithmic law given in equations (56) and (57).

8. *Relation to Slender-body Theory.*—A comparison between the results from linearised theory and from exact calculations has been made in Ref. 1 for wings of infinite aspect ratio. It is of interest to make a similar comparison for wings of very small aspect ratio, in which case the results from slender-body theory for subsonic flow can be taken instead of exact calculations.

We discuss first some points of the slender-body theory. This discussion is based on the work by Adams and Sears[8] (1953). The results are expressed in a more explicit way, which makes it easy to show the relation to the linearised slender-body theory as given by Keune and Oswatitsch[9, 14] (1953) and to the ordinary linear theory.

In slender-body theory it is assumed that the shape of the body and as a consequence the $v_x$-velocity component vary only slowly in the $x$-direction. Therefore, the potential equation

$$\frac{\partial^2\phi}{\partial x^2}+\frac{\partial^2\phi}{\partial y^2}+\frac{\partial^2\phi}{\partial z^2}=0 \qquad (58)$$

at or near the body surface can be written approximately as:

$$\frac{\partial^2\phi}{\partial y^2}+\frac{\partial^2\phi}{\partial z^2}=0\,. \qquad (59)$$

To solve this equation is a two-dimensional problem. The potential function has to be determined so that the boundary condition of zero normal velocity at the body surface is satisfied. For slender bodies the boundary condition can be written in the form :

$$\begin{aligned}\frac{\partial\phi(x,y,z)}{\partial n} &= v_n(y,z;x)=\frac{dn}{dx}(y,z;x)(V_0+v_x)\simeq\frac{dn\,(y,z;x)}{dx}V_0\\ &=\frac{\partial z}{\partial x}\frac{1}{\{1+(\partial z/\partial y)^2\}^{1/2}}V_0 \qquad (60)\end{aligned}$$

where $\partial\phi/\partial n$ is the derivative of $\phi$ taken normal to the boundary of the cross-section $z(y;x)$ in a plane $x =$ constant and where $dn$ is the local normal distance between the two cross-sections at $x+dx$ and $x$ projected into the same transversal plane.

The chordwise ordinate $x$ enters equations (59) and (60) only in the form of a parameter, which means that the potential function can be determined from equations (59) and (60) except for an additive function of $x$. We write, therefore, the potential function in the form

$$\phi(x,y,z)=\phi_1(y,z;x)+\phi_2(x) \qquad (61)$$

where $\phi_1(y,z;x)$ is a velocity potential for two-dimensional flow in the $y,z$-plane which satisfies the condition (60) at the boundary of the cross-section $z(y;x)$.

We determine first the potential $\phi_1(y,z;x)$; the determination of $\phi_2(x)$ will be discussed later. For this purpose, we transform the $\zeta=y+iz$ plane into a $\zeta_1$-plane so that the body cross-section in the $\zeta$-plane is transformed into a circle of radius $r$. Our task is to determine a distribution of singularities inside or on the circumference of the circle which produces a normal velocity component $v_{n1}(\zeta_1)$ which is related to $v_n(\zeta)$ by the mapping ratio $|d\zeta/d\zeta_1|$ :

$$v_{n\,1}(\zeta_1)=v_n(\zeta)\left|\frac{d\zeta}{d\zeta_1}\right|. \qquad (62)$$

We make use of the fact that a source distribution on the circle $\zeta_1=r\,e^{i\vartheta}$ of strength $q(\vartheta)$, with the total strength equal to zero, produces a normal velocity equal to $q(\vartheta)/2$ at each point on the circle. This is a consequence of the fact that for an isolated source and sink of equal strength all circles through the positions of the source and sink are streamlines. The total strength of the source distribution on the circle being zero, we can always combine a source with a sink of equal strength. Thus at any point on the circle only the local source contributes to the normal velocity.

R.A.E. Form 14 C.B.H. 55258

MINISTRY OF AVIATION
ROYAL AIRCRAFT ESTABLISHMENT

JOB No. ..................

SHEET No. .................. DATE ..................

SKETCH FILE No. ..................

$0 < a < \pi$

$$\int_0^{\pi} K \log|(a-x)|\,dx.$$

$$= \int_0^{a-\delta x} K \log|a-x|\,dx$$

$$+ \int_{a-\delta x}^{a+\delta x} K \log|a-x|\,dx$$

$$+ \int_{a+\delta x}^{\pi} K \log|a-x|\,dx$$

$$= -\Big[-(a-x)\log(a-x) - (a-x)\Big]_{X_1}^{X_2}$$

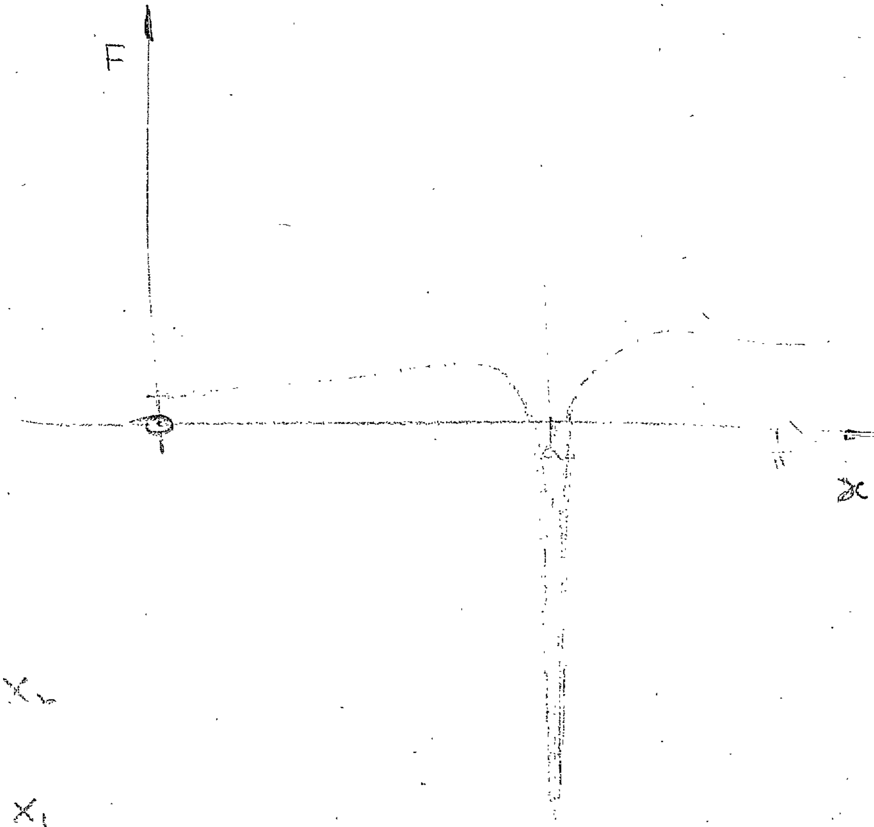


$$\left.\begin{aligned} &= -(\delta x)\log(\delta x) + \cancel{\delta x} + a\log a - a \\ &\quad + \delta x \log(\delta x) - \cancel{\delta x} + \delta x \log \delta x - \cancel{\delta x} \\ &\quad - (a-\pi)\log(a-\pi) + a - \pi + (-\delta x)\log \delta x + \cancel{\delta x} \end{aligned}\right\} \delta x \to 0$$

$$= a\log a - a - (a-\pi)\log(a-\pi) + (a-\pi)$$

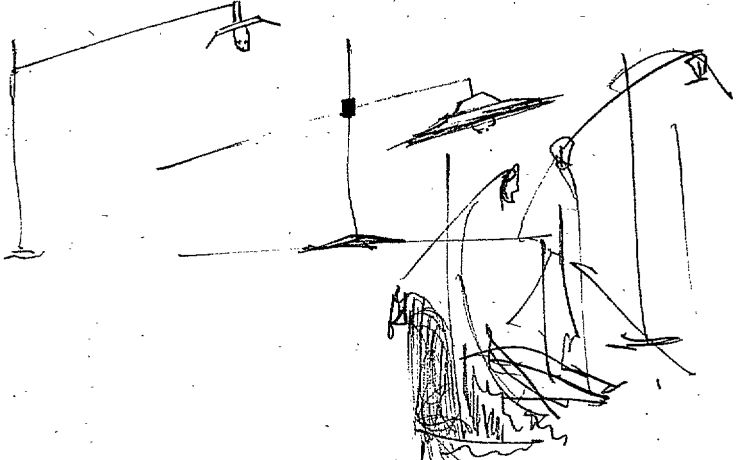

$y_1 = $ a circle.

$\therefore y_1 = r.$

$\log 2|r - y_1'|$

$\log 2(r - r\cos\theta)$

$\log 2r|1 - \cos\theta|$

$\log 2r|(\cos\theta - \cos\theta')|$

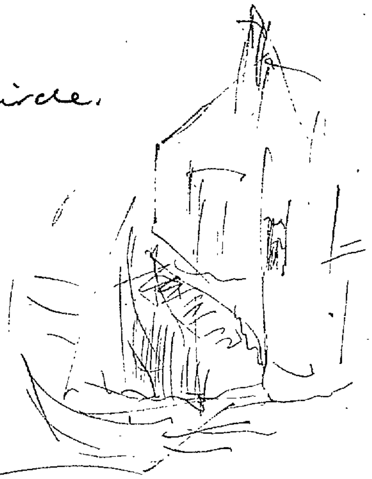

$\int \log(a - x)\,dx$

$-\int \log u\,du. =$

$-[u \log u - u.]$

$= -(a-x)\log(a-x) + (a-x).$

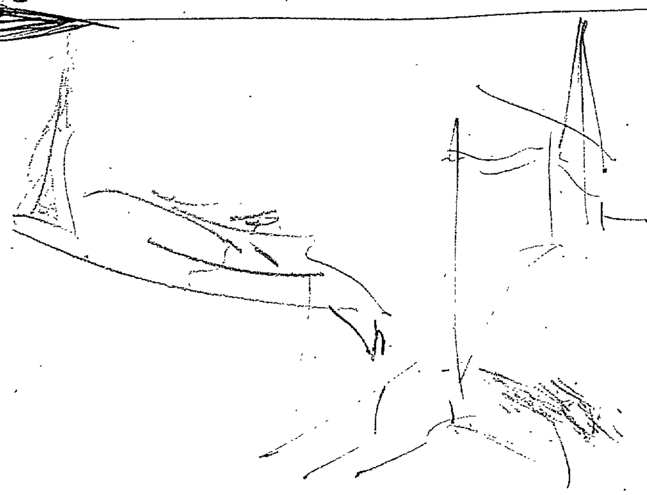

$\cancel{\dfrac{(a-x)}{1/\log(a-x)} \quad \dfrac{-1}{}}$

$\dfrac{\log(a-x)}{1/a-x} = \dfrac{\frac{1}{a-x}}{-\frac{1}{(a-x)^2} \cdot -1.} = (a-x) = 0 \longrightarrow$

R.A.E. Form 14 C.B.H.35258

MINISTRY OF AVIATION

ROYAL AIRCRAFT ESTABLISHMENT

JOB No.

SHEET No. DATE

SKETCH FILE No.

$$\left(\frac{de_1}{de_{11}}\right) = \left[1 - \frac{r^2}{e_1^2}\right]^{1-\frac{2\alpha}{\pi}} \left[1 + \frac{r^2}{e_1^2}\right]^{\frac{2\alpha}{\pi}}$$

$e_1 = r e^{j\theta}$

$$= \left[1 - \frac{1}{e^{2j\theta}}\right]^{1-\frac{2\alpha}{\pi}} \left[1 + \frac{1}{e^{2j\theta}}\right]^{\frac{2\alpha}{\pi}}$$

$$= \left(e^{2j\theta} - 1\right)^{1-\frac{2\alpha}{\pi}} \left(1 + e^{2j\theta}\right)^{\frac{2\alpha}{\pi}} \cdot e^{-2j\theta}$$

$$\frac{e^{j\theta} - e^{-j\theta}}{2}$$

$$\frac{e^{2j\theta} - 1}{2e^{j\theta}}$$

$$= \left(e^{2j\theta} - 1\right)\left(e^{2j\theta} - 1\right)^{-\frac{2\alpha}{\pi}} \left(1 + e^{2j\theta}\right)^{\frac{2\alpha}{\pi}} e^{-2j\theta}$$

$$= \frac{(\sin\theta)^{1-\frac{2\alpha}{\pi}}}{(e^{j\theta})^{1-\frac{2\alpha}{\pi}}} \cdot \frac{(\cos\theta)^{\frac{2\alpha}{\pi}}}{(e^{j\theta})^{\frac{2\alpha}{\pi}}}$$

$$= (\sin\theta)^{1-\frac{2\alpha}{\pi}} (\cos\theta)^{\frac{2\alpha}{\pi}} \cdot e^{-j\theta}$$

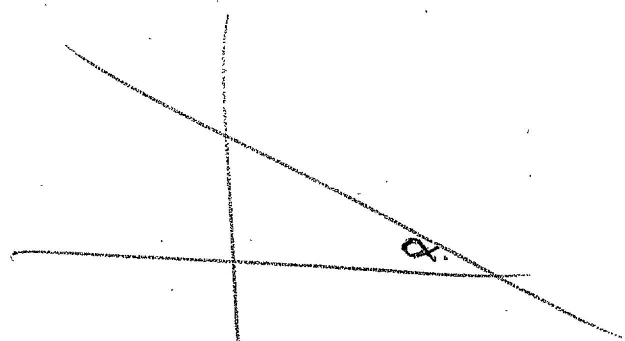


$$\boxed{\frac{de_1}{de_1}} = \cancel{(\sin\theta)(} = (\sin\theta)^{1-\frac{2\alpha}{\pi}} \cdot (\cos\theta)^{\frac{2\alpha}{\pi}} \cdot 1.$$

$y = r \cancel{\cos}\ \theta.$

| ① | ② | ③ | ④ | ②③④ | |
|---|---|---|---|---|---|
| $\theta$ | $v_n(e_0.)$ | $\left\|\frac{de_1}{de_1'}\right\|$. | $\log 2\|y_1-y_1'\|$. | | |
| $0$ | a/c | $(\sin\theta)^{1-\frac{2\alpha}{\pi}}(\cos\theta)^{\frac{2\alpha}{\pi}}$ | $\log 2r\|\alpha^\theta \cos\theta\|$ | | |
| 10 | d/c | | | | |
| 20 | d/c. | | | | |
| 30 | d/c | | | | |
| 40 | d/c | | | | |
| 50 | d/c | | | | |
| 60 | d/c | | | | |
| 70 | d/c | | | | |
| 80 | d/c | | | | |
| 90. | 3/c. | | | | |
| 100 | d/c | | | | |
| 110 | d/c | | | | |
| 120 | d/c | | | | |
| 130 | d/c | | | | |
| 140 | d/c | | | | |
| 150 | d/c | | | | |
| 160 | d/c | | | | |
| 170 | d/c | | | | |
| 180. | a/c. | | | | |

$$\phi_1 = \frac{r}{\pi}\int_0^{\pi} v_{n_1}(\theta')\,\log.\,2\,|(y_1 - y_1')|\,d\theta'.$$

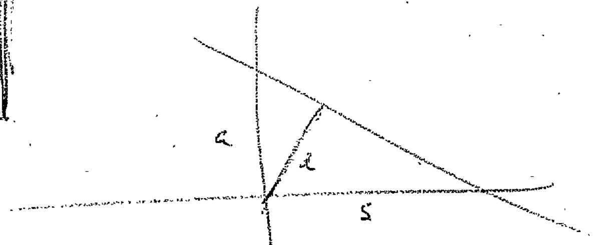


$$v_{n_1}\,e_1' = v_n(e)\left|\left(\frac{de_1}{de_{11}}\right)\right|$$

$$\left|\frac{de}{de_1}\right| = 2\left[1 - \frac{r^2}{e_1^2}\right]^{1-\frac{2\alpha}{\pi}}\left[1 + \frac{r^2}{e_1^2}\right]^{\frac{2\alpha}{\pi}}$$

| $\theta$ | $v_n(e)$ | $\left\lvert\frac{de_1}{de_{11}}\right\rvert$ | $\log 2\lvert y_1 - y_1'\rvert$ |
|---|---|---|---|
| 0 | $a/c$. | 0. | |
| 10 | | | |
| 20 | | | |
| 30 | $d/c$ | | |
| 40 | | | |
| 50 | | | |
| 60 | | | |
| 70 | | | |
| 80 | | | |
| 90 | $s/c$ | | |

$$e_1 = r e^{j\theta}$$

$$\left(\frac{de_1}{de_{11}}\right) = \frac{2\left(e^{j\theta} - 1\right)^{1-\frac{2\alpha}{\pi}}\left(e^{j\theta}+1\right)^{\frac{2\alpha}{\pi}}}{e^{j\theta}}$$

$$= \frac{\left(e^{j\theta}-1\right)^{1-\frac{2\alpha}{\pi}}\left(e^{j\theta}+1\right)^{\frac{2\alpha}{\pi}}}{e^{j\theta}}$$

$$\int \log(a-x)\,dx$$

$$= -\int \log u \, du$$

$$= -u \log u + u$$

$$= -(a-x)\log(a-x) + (a-x)$$

$$x \to a$$

$$\frac{\log(a-x)}{\frac{1}{(a-x)}} = \frac{-\frac{1}{(a-x)}}{-\frac{1}{(a-x)^2}} = (a-x) \to 0$$

$$\log 2r\,|(\cos\theta - \cos\theta')|$$

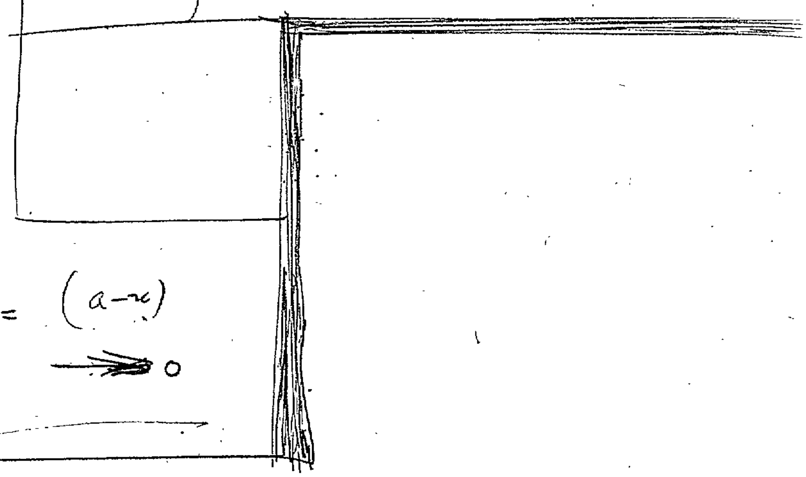

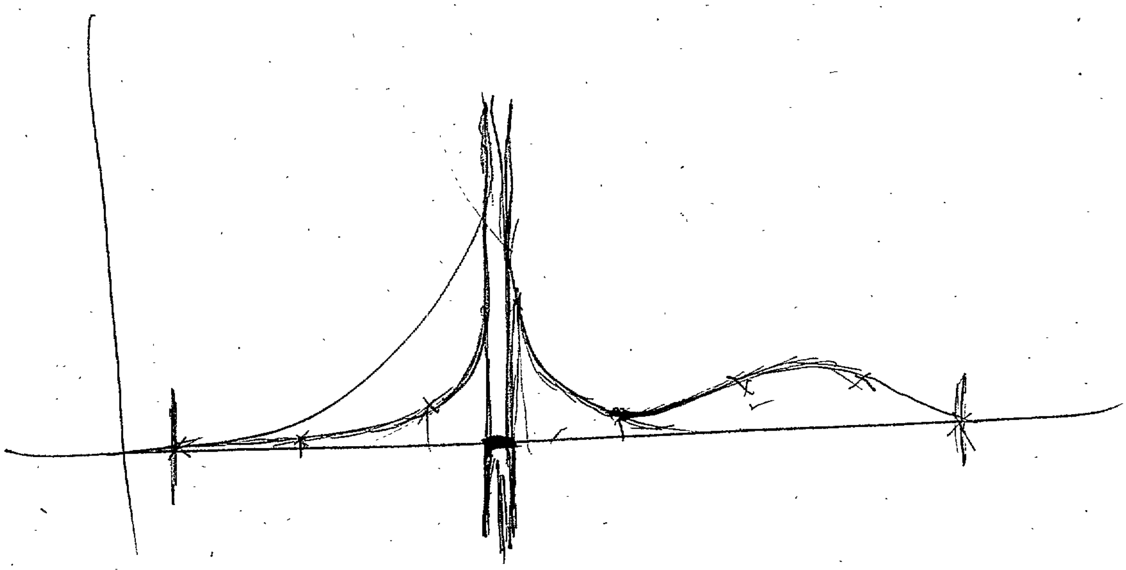

$$\left[\frac{dl}{dl_1}\right] = \left[1 - \frac{r^2}{l_1^2}\right]^{1-\frac{2\alpha}{\pi}}\left[1+\frac{r^2}{l_1^2}\right]^{\frac{2\alpha}{\pi}} \qquad (1)$$

$l_1 = re^{j\theta}$ in the reqd circle.

$$v_{n'}(l_1) = v_n(l)\left|\frac{dl}{dl_1}\right| \qquad (2)$$

$v_n(l)$ is known $= f(\theta)$. (3)

$$\therefore v_{n'}(l_1) = f(\theta)\left[1 - \frac{r^2}{l_1^2}\right]^{1-\frac{2\alpha}{\pi}}\left[1+\frac{r^2}{l_1^2}\right]^{\frac{2\alpha}{\pi}} \qquad (4)$$

$$\phi_1 = \frac{r}{\pi}\int_0^\pi v_{n'}(\theta')\log.2.|y_1 - y_1'|\,d\theta' \qquad (5).$$

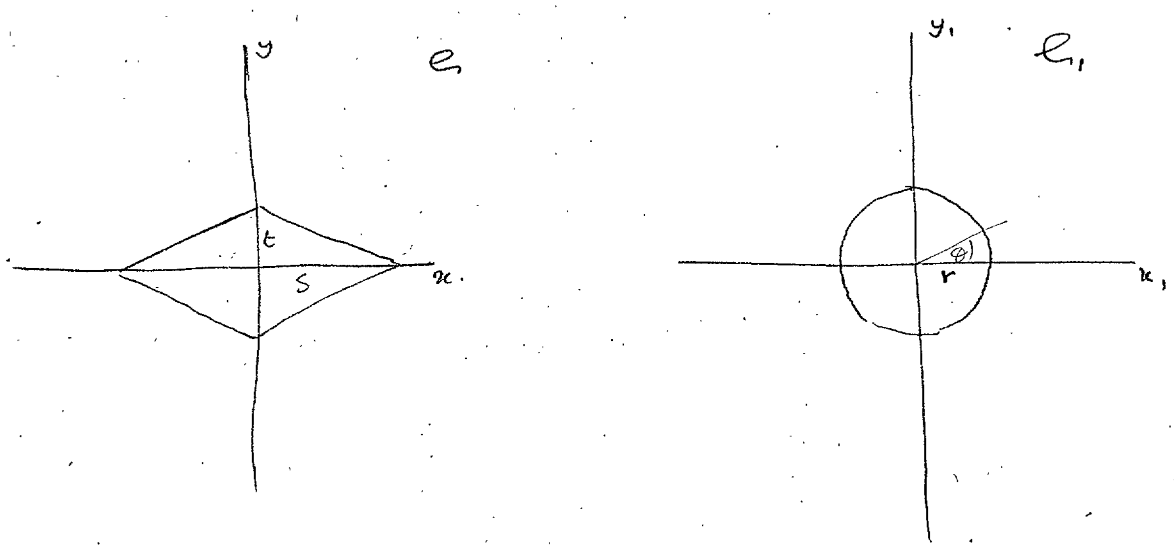


$$\phi_1 = \frac{r}{\pi}\int_0^\pi f(\theta')\times\left[1 - \frac{r^2}{l_1'^2}\right]^{1-\frac{2\alpha}{\pi}}\left[1+\frac{r^2}{l_1'^2}\right]^{\frac{2\alpha}{\pi}}\times\log.2.|y_1 - y_1'|\,d\theta' \qquad (6)$$

$$\phi_1 = \frac{r}{\pi}\int_0^\pi f(\theta')\left[1 - \frac{r^2}{l_1'^2}\right]^{1-\frac{2\alpha}{\pi}}\left[1+\frac{r^2}{l_1'^2}\right]^{\frac{2\alpha}{\pi}}\times\log 2.|\eta_1 - \eta_1'|\,d\theta'$$

$$+\frac{r}{\pi}\int_0^\pi f(\theta')\left[1 - \frac{r^2}{l_1'^2}\right]^{1-\frac{2\alpha}{\pi}}\left[1+\frac{r^2}{l_1'^2}\right]^{\frac{2\alpha}{\pi}}.\log.s(x).\,d\theta' \qquad (7).$$

$$\phi_1 = \frac{r}{\pi}\int_0^{\pi} v_{n1}(\theta')\,\log 2\,|y_1 - y_1'|\,d\theta'$$

$$v_{n1}(\zeta_1) = v_n(\zeta)\left|\frac{d\zeta}{d\zeta_1}\right|$$

Reqd cross section is in $\zeta$ plane. Transformed into a circle in the $\zeta_1$ plane.

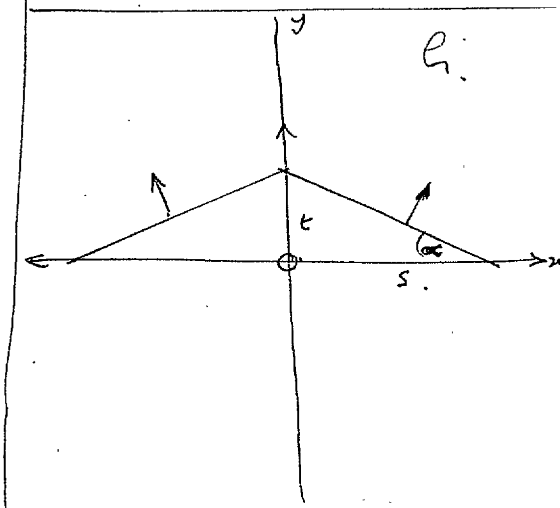


$$v_n(\zeta_1) = f(\theta)$$

| | |
|---|---|
| $\theta = 0$ | $v_n(\zeta_1) = s/c$ |
| $0 < \theta < \pi/2$ | $v_n(\zeta_1) = s/c \sin\alpha$ |
| $\theta = \pi/2$ | $v_n(\zeta_1) = t/c$ |
| $\pi/2 < \theta < \pi$ | $v_n(\zeta_1) = \frac{s}{c}\sin\alpha$ |
| $\theta = \pi$ | $v_n(\zeta_1) = s/c$ |

<u>Conformal transformation of rhombus into circle.</u>

$$\left(\frac{d\zeta}{dz}\right) = \left(1 - \frac{a^2}{z^2}\right)^{1-n}\left(1 + \frac{a^2}{z^2}\right)^{n}$$

$a$ = radius of circle.

$\frac{n\pi}{2} = \alpha$.

$n = \frac{2\alpha}{\pi}$

$$\therefore v_{n1}(\zeta_1) = v_n(\zeta)\left|\left(1 - \frac{a^2}{z^2}\right)^{1-n}\left(1 + \frac{a^2}{z^2}\right)^{n}\right|$$

$$= v_n(\zeta)\left|\left(1 - \frac{a^2}{z^2}\right)^{1-\frac{2\alpha}{\pi}}\left(1 + \frac{a^2}{z^2}\right)^{2\alpha/\pi}\right|$$

$$\therefore \phi_1 = \frac{r}{\pi}\int_0^{\pi} v_n(\zeta)\left|\left(1 - \frac{r^2}{\zeta_1^2}\right)^{1-\frac{2\alpha}{\pi}}\left(1 + \frac{r^2}{\zeta_1^2}\right)^{\frac{2\alpha}{\pi}}\right|\log.2.|y_1 - y_1'|\,d\theta'$$

$$\phi_1 = \frac{r}{\pi}\int_0^{\pi} f(\theta)\left|\left(1 - \frac{r^2}{\zeta_1^2}\right)^{1-\frac{2\alpha}{\pi}}\left(1 + \frac{r^2}{\zeta_1^2}\right)^{\frac{2\alpha}{\pi}}\right|\log.2.|y_1 - y_1'|\,d\theta'$$

Since a single source of strength $Q$ at the centre of the circle produces at the circle the normal velocity

$$v_n = \frac{Q}{2\pi r}$$

the required normal velocities $v_{n\,1}$ on the circle $\zeta_1 = r\,e^{i\vartheta}$ are produced by a single source at the centre of the circle of strength:

$$Q(x) = r\int_0^{2\pi} v_{n\,1}(\vartheta')\,d\vartheta' = 2\pi r\bar{v}_{n\,1} \quad \ldots \quad (63)$$

and a source distribution on the circle of strength:

$$q(\vartheta) = 2(v_{n\,1} - \bar{v}_{n\,1}) \,. \quad \ldots \quad (64)$$

The potential of the single source and the source distribution on the circle and also therefore at the body surface is:

$$\phi_1(\zeta_1) = \phi_1(\zeta) = \frac{Q}{2\pi}\ln r + \frac{r}{2\pi}\int_0^{2\pi} q(\vartheta')\ln|\zeta_1 - \zeta_1'|\,d\vartheta' \,. \quad \ldots \quad (65)$$

By equations (62) to (64) :

$$\begin{aligned}\phi_1 &= r\bar{v}_{n\,1}\ln r + \frac{r}{\pi}\int_0^{2\pi}(v_{n\,1} - \bar{v}_{n\,1})\ln|\zeta_1 - \zeta_1'|\,d\vartheta' \\ &= r\bar{v}_{n\,1}\left[\ln r - \frac{1}{\pi}\int_0^{2\pi}\ln|\zeta_1 - \zeta_1'|\,d\vartheta'\right] \\ &\quad + \frac{r}{\pi}\int_0^{2\pi} v_{n\,1}\ln|\zeta_1 - \zeta_1'|\,d\vartheta' \,. \quad \ldots \quad (66)\end{aligned}$$

On the circle

$$\begin{aligned}\zeta_1 &= r(\cos\vartheta + i\sin\vartheta) \\ \zeta_1' &= r(\cos\vartheta' + i\sin\vartheta') \\ \int_0^{2\pi}\ln|\zeta_1 - \zeta_1'|\,d\vartheta' &= 2\pi\ln r + \pi\ln 2 + \tfrac{1}{2}\int_0^{2\pi}\ln[1 - \cos(\vartheta - \vartheta')]\,d\vartheta' \\ &= 2\pi\ln r \,. \quad \ldots \quad (67)\end{aligned}$$

From equations (63), (66) and (67):

$$\phi_1 = \frac{r}{\pi}\int_0^{2\pi} v_{n\,1}(\vartheta')[\ln|\zeta_1 - \zeta_1'| - \tfrac{1}{2}\ln r]\,d\vartheta' \,.$$

We consider only thickness effects here, which implies that the cross-sections are symmetrical about the $y$-axis and $v_{n\,1}(\vartheta') = v_{n\,1}(-\vartheta')$. Therefore,

$$\begin{aligned}\phi_1 &= \frac{r}{\pi}\int_0^{\pi} v_{n\,1}(\vartheta')[\ln|\zeta_1 - \zeta_1'| + \ln|\zeta_1 - \bar{\zeta}_1'| - \ln r]\,d\vartheta' \\ &= \frac{r}{\pi}\int_0^{\pi} v_{n\,1}(\vartheta')[\tfrac{1}{2}\ln(\zeta_1 - \zeta_1')(\bar{\zeta}_1 - \bar{\zeta}_1')(\zeta_1 - \bar{\zeta}_1')(\bar{\zeta}_1 - \zeta_1') - \ln r]\,d\vartheta' \\ &= \frac{r}{\pi}\int_0^{\pi} v_{n\,1}(\vartheta')[\ln 2r|y_1 - y_1'| - \ln r]\,d\vartheta' \\ &= \frac{r}{\pi}\int_0^{\pi} v_{n\,1}(\vartheta')\ln 2|y_1 - y_1'|\,d\vartheta' \,. \quad \ldots \quad (68)\end{aligned}$$

If the conformal transformations of the body cross-sections into a circle and the required normal velocities are known, equations (62) and (68) determine the potential $\phi_1(y,z;x)$, with $x$ entering as a parameter.

To demonstrate more clearly the relation to linear theory, we transform the $\zeta_1$-plane into the $\zeta_2$-plane so that the circle is transformed into a slit:

$$\zeta_2 = \zeta_1 + \frac{r^2}{\zeta_1}. \qquad \ldots \qquad (69)$$

With

$$v_{n\,2}(y_2') = v_{n\,1}(\vartheta') \frac{1}{\left|\frac{d\zeta_2}{d\zeta_1}\right|} = \frac{v_{n\,1}(\vartheta')}{2|\sin\vartheta'|}$$

$$y_2' = 2r\cos\vartheta' = 2y_1'$$

and

$$dy_2' = -2r\, sin\,\vartheta'\, d\vartheta'$$

we obtain:

$$\phi_1 = \frac{1}{\pi}\int_{-s_2(x)}^{+s_2(x)} v_{n\,2}(y_2') \ln|y_2 - y_2'|\, dy_2'.$$

Since

$$v_{n\,2}(y_2') = v_n(y')\left|\frac{d\zeta}{d\zeta_2}\right| = v_n(y')\frac{d\sigma'}{dy_2'}$$

$$= v_n(y')\left\{1 + \left(\frac{\partial z}{\partial y}\right)^2_{y=y'}\right\}^{1/2}\frac{dy'}{dy_2'}$$

$$= \frac{\partial z}{\partial x}(y')\frac{dy'}{dy_2'}V_0$$

where $\sigma$ is the length of arc along the circumference of the body cross-section, we obtain finally for the potential $\phi_1$:

$$\phi_1(y,z;x) = \frac{V_0}{\pi}\int_{-s(x)}^{+s(x)}\frac{\partial z(y';x)}{\partial x}\ln|y_2(y) - y_2(y')|\, dy'. \qquad \ldots \qquad (70)$$

The determination of $\phi_1(y,z;x)$ by equations (68) or (70) is in most cases rather laborious. Keune[9] has therefore derived an approximate method by introducing into the slender-body theory the simplifications of linear theory. He replaces equation (70) by the following:

$$\phi_1(y,z;x) = \frac{V_0}{\pi}\int_{-s(x)}^{s(x)}\frac{\partial z(x,y')}{\partial x}\ln\{(y-y')^2 + z^2\}^{1/2}\, dy' \qquad \ldots \qquad (71)$$

and puts $z$ equal to zero everywhere as long as no singular behaviour occurs. This means that the same source distribution as in ordinary linear theory is taken and placed in the chordal plane. In both methods the potential and hence the velocity are also calculated in the chordal plane. These simplifications are justifiable for bodies where the thickness of the cross-sections is small compared with their spanwise extension, and away from rounded tips.

To determine the function $\phi_2(x)$ in equation (61) one has to return to the complete potential equation (58) and satisfy the additional boundary condition $\phi(x,y,z) = \partial\phi(x,y,z)/\partial x = 0$ at infinity. This calculation was carried out, *e.g.*, by Adams and Sears[8]. They derived the following equation for the function $\phi_2(x)$:

$$\phi_2(x) = \frac{V_0}{2\pi}\Big[S'(x)\ln\frac{\beta}{2} - \tfrac{1}{2}S'(0)\ln x - \tfrac{1}{2}S'(1)\ln(1-x)$$
$$- \tfrac{1}{2}\int_0^x S''(x')\ln(x-x')\, dx' + \tfrac{1}{2}\int_x^1 S''(x')\ln(x'-x)\, dx'\Big] \qquad \ldots \qquad (72)$$

where $S(x)$ is the cross sectional area of the body at the position $x$ and $S'(x)$ and $S''(x)$ the derivatives with respect to $x$.

This result can be explained by the following considerations. The body can be represented by a source distribution $q(x,y,z)$, whose strength, for slender bodies, is equal in each transverse plane, to that of the two-dimensional sources—extending from infinity downstream to infinity upstream—determined above, so as to give the required flow in the planes $x =$ constant. The function $\phi_2(x)$ does not depend on $y$ and $z$, *i.e.*, it is not affected by the actual shape of the cross-sections. It depends only on the total source strength at each position $x$ and not on the way in which the sources are distributed in each transverse plane. The function $\phi_2$ can therefore be determined as that for a body of revolution which has the same cross-sectional area $S(x)$ at each position $x$ as the given wing or body.

For slender bodies of revolution the total velocity potential is given by the relation:

$$\phi(x,r) = -\frac{V_0}{4\pi}\int_0^1 \frac{S'(x')\,dx'}{\{(x-x')^2+\beta^2 r^2\}^{1/2}} \qquad (73)$$

This formula is derived by replacing the body by a distribution of three-dimensional sources along the axis and using the Prandtl-Glauert analogy between compressible and incompressible flow. We determine $\phi_2(x)$ as the difference between $\phi(x,r)$ and $\phi_1(x,r)$. Since the cross-sections in transverse planes are circles, the potential $\phi_1(y,z;x)$ is:

$$\begin{aligned}\phi_1(y,z;x) &= \frac{Q(x)}{2\pi}\ln r(x)\\ &= \frac{V_0}{2\pi}S'(x)\ln r(x)\,. \end{aligned} \qquad (74)$$

Thus,

$$\phi_2(x) = -\frac{V_0}{4\pi}\int_0^1 \frac{S'(x')\,dx'}{\{(x-x')^2+\beta^2 r^2\}^{1/2}} - \frac{V_0}{2\pi}S'(x)\ln r$$

$$= -\frac{V_0}{4\pi}\left\{S'(x)\int_0^1 \frac{dx'}{\{(x-x')^2+\beta^2 r^2\}^{1/2}} + \int_0^1 \frac{S'(x')-S'(x)}{\{(x-x')^2+\beta^2 r^2\}^{1/2}}\,dx' + 2S'(x)\ln r\right\}.$$

The integrand of the second integral vanishes for $x = x'$ and for $x \neq x'$ the term $\beta^2 r^2$ can be ignored.

Therefore

$$\phi_2(x) = -\frac{V_0}{4\pi}\left\{S'(x)\int_0^x \frac{d(x-x')}{\{(x-x')^2+\beta^2 r^2\}^{1/2}} + S'(x)\int_0^{1-x} \frac{d(x'-x)}{\{(x'-x)^2+\beta^2 r^2\}^{1/2}}\right.$$

$$\left. + \int_0^x \frac{S'(x')-S'(x)}{x-x'}\,dx' + \int_x^1 \frac{S'(x')-S'(x)}{x'-x}\,dx' + 2S'(x)\ln r\right\}$$

and finally we obtain equation (72) for $\phi_2$.

Keune has arrived at equation (72) by making the approximations of slender-body theory in the expression for the velocity potential corresponding to the source distribution from linear theory.

The streamwise velocity component is calculated by differentiating $\phi(x,y,z)$ with respect to $x$.

Since $\phi_1(y,z;x)$ does not vary with Mach number, from equations (61) and (72) we obtain the logarithmic law of equation (57) for the variation of the velocity with Mach number.

The linearised slender-body theory of Keune and Oswatitsch is not identical with the linear theory as used in the previous sections. The same source distribution is used in both methods but the streamwise velocity increment is calculated differently. Both methods intend to calculate the velocity which the source distribution produces in the chordal plane. This is done correctly in the ordinary linear theory, whilst in Keune's method the assumptions of slender-body theory are made. The differences of course become smaller the more these assumptions are justified, *i.e.*, with decreasing aspect ratio. Keune has shown that for the centre-section of rectangular wings with biconvex section the results from linearised slender-body theory agree with those of the straightforward linear theory up to aspect ratio 0·4. In the next section we will compare the results of the various methods with the exact solution for ellipsoids which have three different axes.

9. *The Velocity Distribution on Ellipsoids Determined by Various Methods*.—To show the effect of the simplifications of linear theory and slender-body theory on the velocity distribution we calculate the velocities on ellipsoids by slender-body theory, linearised slender-body theory and ordinary linear theory. Though neither the assumptions of slender-body theory nor those of linear theory hold near the nose of ellipsoids, we choose the ellipsoids since these are one of the few cases where an exact solution exists, *see* Refs. 15 and 16. The comparison of the approximate results with the exact results will give a range of values of the span through which the application of slender-body theory is permissible.

Let the thickness of the ellipsoid be $t$, and the largest spanwise extent $2s$. All lengths are made dimensionless with the length of the ellipsoid. The ellipsoid may be represented by the equation

$$z(x,y) = \frac{t}{2}\left\{1 - (1-2x)^2 - (y/s)^2\right\}^{1/2}. \qquad (75)$$

The elliptic cross-sections are transformed into circles of radius $r$ by the transformation

$$\zeta = \zeta_1 + \frac{R^2}{\zeta_1} \qquad (76)$$

with

$$r = \frac{2s+t}{4}\left\{1 - (1-2x)^2\right\}^{1/2} \qquad (77)$$

$$R = \frac{(4s^2 - t^2)^{1/2}}{4}\left\{1 - (1-2x)^2\right\}^{1/2}. \qquad (78)$$

By equations (60), 75 and (76) the normal velocity $v_n(\zeta)$ is:

$$v_n(\zeta) = ts\,\frac{1-2x}{\{1-(1-2x)^2\}^{1/2}}\,\frac{1}{\{s^2\sin^2\vartheta + (t/2)^2\cos^2\vartheta\}^{1/2}}\,V_0 \qquad (79)$$

where $\zeta_1 = re^{i\vartheta}$ is the circle in the $\zeta_1$-plane. For points on the circle, the mapping ratio is:

$$\left|\frac{d\zeta}{d\zeta_1}\right| = \left|1 - \frac{R^2}{r^2}\,\mathrm{e}^{-2i\vartheta}\right| = \left\{1 - 2\frac{R^2}{r^2}\cos 2\vartheta + \frac{R^4}{r^4}\right\}^{1/2}$$

$$= \frac{4}{2s+t}\left\{s^2\sin^2\vartheta + (t/2)^2\cos^2\vartheta\right\}^{1/2}. \qquad (80)$$

By equations (79) and (80) we obtain the normal velocity $v_{n1}$ at the circle:

$$v_{n1} = \frac{4ts}{2s+t}\,\frac{1-2x}{\{1-(1-2x)^2\}^{1/2}}\,V_0\,, \qquad (81)$$

*i.e.*, a constant value along the circumference of the circle. The boundary condition (81) can be satisfied by placing a single source of strength $Q(x)$ at the centre:

$$Q(x) = 2\pi r(x) v_{n1}(x)$$

$$= 2\pi ts(1-2x)V_0\,. \qquad (82)$$

The potential $\phi_1(y,z;x)$ is therefore:

$$\begin{aligned}\phi_1(y,z;x) &= \frac{Q(x)}{2\pi} \ln r(x) \\ &= V_0 ts(1-2x) \ln \left[\frac{2s+t}{4}\left\{1-(1-2x)^2\right\}^{1/2}\right] \\ &= V_0 ts(1-2x)\left\{\ln \frac{2s+t}{4} + \tfrac{1}{2}\ln 4x(1-x)\right\}. \qquad (83)\end{aligned}$$

Since $\quad S(x) = \pi \dfrac{t}{2} s[1-(1-2x)^2]$

we obtain by equation (72):

$$\phi_2(x) = V_0 ts(1-2x)\{1 - \tfrac{1}{2}\ln 4x(1-x)\}. \qquad (84)$$

The total potential is then:

$$\phi(x,y,z) = V_0 ts(1-2x)\left\{1 + \ln \frac{2s+t}{4}\right\} \qquad (85)$$

and the streamwise velocity increment is

$$v_x = \phi_x(x,y,z) = V_0 2ts\left\{\ln \frac{2}{s+t/2} - 1\right\}. \qquad (86)$$

The velocity increment from slender-body theory is thus constant along the whole surface, as was the velocity from linear theory for the two-dimensional wing with elliptic cross-section.

By linearised slender-body theory, *i.e.*, by equation (71), we obtain for the potential $\phi_1$ at the plane of symmetry:

$$\begin{aligned}\phi_1(x,0,0) &= \frac{2}{\pi} V_0 \int_0^{s(x)} \frac{t(1-2x)}{\{1-(1-2x)^2-(y'/s)^2\}^{1/2}} \ln y' \, dy' \\ &= \frac{2st(1-2x)}{\pi} V_0 \int_0^1 \frac{\ln y'}{\left\{1-\left[\dfrac{y'}{s\{1-(1-2x)^2\}^{1/2}}\right]^2\right\}^{1/2}} d\left[\frac{y'}{s\{1-(1-2x)^2\}^{1/2}}\right] \\ &= \frac{2st(1-2x)}{\pi} V_0 \left[\ln s\{1-(1-2x)^2\}^{1/2} \int_0^1 \frac{d\tau}{(1-\tau^2)^{1/2}} + \int_0^1 \frac{\ln \tau}{(1-\tau^2)^{1/2}} d\tau\right] \\ &= V_0 ts(1-2x)\{\ln s\{1-(1-2x)^2\}^{1/2} - \ln 2\} \\ &= V_0 ts(1-2x)\left\{\ln \frac{s}{2} + \tfrac{1}{2}\ln 4x(1-x)\right\}. \qquad (87)\end{aligned}$$

Thus the potentials $\phi_1$ from slender-body theory and linearised slender-body theory differ by the term

$$V_0 ts(1-2x) \ln\left(1+\frac{t}{2s}\right).$$

This difference is the same for all spanwise stations, as follows from the relations:

$$\begin{aligned} y &= s\{1-(1-2x)^2\}^{1/2}\cos\vartheta \\ &= 2r\cos\vartheta \cdot \frac{1}{1+t/2s} \\ &= 2y_1 \cdot \frac{1}{1+t/2s} \\ &= y_2 \cdot \frac{1}{1+t/2s}. \qquad (88)\end{aligned}$$

The potential $\phi_1$ from general slender-body theory is by equations (70) and (88):

$$\phi_1(y,z;x) = \frac{V_0}{\pi}\int_{-s(x)}^{s(x)} \frac{\partial z(y';x)}{\partial x} \ln\left|(y-y')\left(1+\frac{t}{2s}\right)\right| dy'$$

$$= \frac{V_0}{\pi}\int_{-s(x)}^{s(x)} \frac{\partial z(y';x)}{\partial x} \ln|y-y'|\, dy'$$

$$+ \frac{V_0}{\pi}\ln\left(1+\frac{t}{2s}\right)\int_{-s(x)}^{s(x)} \frac{\partial z(y';x)}{\partial x}\, dy' . \qquad (89)$$

The first integral in equation (89) is the value for $\phi_1$ from linearised theory and the second term is independent of $y$ and equal to

$$V_0 ts(1-2x)\ln\left(1+\frac{t}{2s}\right).$$

The function $\phi_2$, being the same for linearised and general slender-body theory, is again given by equation (84). Therefore for the streamwise velocity component we obtain the equation:

$$v_x(x,y,0) = V_0 2ts\left[\ln\frac{2}{s} - 1\right]. \qquad (90)$$

The difference from the value given by general slender-body theory is

$$V_0 2ts \ln\left(1+\frac{t}{2s}\right)$$

which, for small values of $t/2s$, is equal to $V_0 t^2$ *.

Next, we calculate the velocity on the ellipsoid by ordinary linear theory, equations (1) and (2). For points on the section of symmetry:

$$\frac{v_x(x,0,0)}{V_0} = \frac{t}{\pi}\int_0^1 dx' \int_0^{s(x')} \frac{1-2x'}{\{1-(1-2x')^2-(y'/s)^2\}^{1/2}} \frac{x-x'}{\{(x-x')^2+y'^2\}^{3/2}}\, dy' \qquad (91)$$

The integration over $y$ leads to a complete elliptic integral of the second kind $\mathbf{E}(k)$.

$$\frac{v_x(x,0,0)}{V_0} = \frac{ts}{\pi}\int_0^1 \frac{1-2x'}{x-x'} \frac{\mathbf{E}(k)}{\{(x-x')^2+s^2[1-(1-2x')^2]\}^{1/2}}\, dx' \qquad (92)$$

with $$k^2 = \frac{s^2[1-(1-2x')^2]}{(x-x')^2+s^2[1-(1-2x')^2]} . \qquad (93)$$

For the mid-chord point, $x = 0\cdot5$, we get

$$\frac{v_x(0\cdot5,0,0)}{V_0} = \frac{2ts}{\pi}\int_0^1 \frac{\mathbf{E}(k)}{\{s^2+(\frac{1}{4}-s^2)(1-2x')^2\}^{1/2}}\, dx' \qquad (94)$$

with $$k^2 = \frac{s^2[1-(1-2x')^2]}{s^2+(\frac{1}{4}-s^2)(1-2x')^2} . \qquad (95)$$

---

* For all values of $t/2s$ one obtains the correction term $-t^2V_0$, to be included in equation (90), by application of the second approximation derived by Keune in Ref. 17. Keune takes into account the differences between the velocities which a source distribution in the chordal plane induces, either at the wing surface or at the chordal plane, by expanding the velocity components in Taylor series with respect to $z$, and ignoring the higher-order terms.

Finally, we calculate the exact velocity on ellipsoids. It has been shown, *see e.g.*, Lamb[15], and Maruhn[16] (1941) that the velocity at the surface of ellipsoids is given by the equation:

$$\frac{V(x,y,z(x,y))}{V_0} = C\left\{1 - \frac{(2x-1)^2}{(2x-1)^2 + [1-(2x-1)^2]\left[\dfrac{\cos^2\psi}{4s^2} + \dfrac{\sin^2\psi}{t^2}\right]}\right\}^{1/2} \quad \ldots \quad (96)$$

where $C$ is the velocity at any point at the mid-chord section of the ellipsoid:

$$C = \frac{V[0{\cdot}5,y,z(0{\cdot}5,y)]}{V_0} = \frac{2}{2-\alpha_0}$$

and
$$\alpha_0 = 2ts\int_0^\infty \frac{d\lambda}{\{(1+\lambda)^3(t^2+\lambda)(4s^2+\lambda)\}^{1/2}}. \quad \ldots \quad (97)$$

$\psi$ is the angle of intersection of the $x,y$-plane and the plane through the line of symmetry $y = z = 0$ and the point $x,y,z$ on the ellipsoid.

By the transformation

$$u = \frac{1}{1+\lambda}$$

$\alpha_0$ can be written as an elliptic integral of the second kind :

$$\alpha_0 = \frac{2ts}{\{(1-t^2)(1-4s^2)\}^{1/2}}\int_0^1 \frac{u\,du}{\left\{u\left(u-\dfrac{1}{1-t^2}\right)\left(u-\dfrac{1}{1-4s^2}\right)\right\}^{1/2}} \quad \ldots \quad (98)$$

which can be expressed by Legendre's standard integrals of the first and second kind $F(\varphi,k)$ and $E(\varphi,k)$ (*see* Ref. 18, p. 76).

$$\int \frac{u\,du}{\{u(u-\alpha_1)(u-\alpha_2)\}^{1/2}} = \frac{a(ad-bc)}{c\gamma}F(\varphi,k)$$
$$-\frac{(ad-bc)^2}{c\gamma}\left[\frac{k\cos\varphi\{1-k^2\sin^2\varphi\}^{1/2}}{(1-k^2)(1+k\sin\varphi)} + \frac{1}{1-k^2}E(\varphi,k)\right] \quad \ldots \quad (99)$$

where
$$k = \frac{\sqrt{\alpha_1} - \sqrt{(\alpha_1-\alpha_2)}}{\sqrt{\alpha_1} + \sqrt{(\alpha_1-\alpha_2)}}$$

$$a = k[\alpha_1 + \sqrt{\{\alpha_1(\alpha_1-\alpha_2)\}}]$$

$$b = \alpha_1 - \sqrt{\{\alpha_1(\alpha_1-\alpha_2)\}}$$

$$c = k$$

$$d = 1$$

$$\gamma = \sqrt{\{\alpha_1(\alpha_1-\alpha_2)\}}[\sqrt{\alpha_1} - \sqrt{\{\alpha_1-\alpha_2\}}]$$

$$u = \frac{a\sin\varphi + b}{c\sin\varphi + d}.$$

The relation between the velocity at any point on the ellipsoid and the velocity at mid-chord, equation (96), can be expressed by means of the local slope in a plane $\psi = \text{const.}$ Let $r$ be the distance of the point $x,y,z$ on the ellipsoid from the point $x,y = 0$, $z = 0$ on the axis, and $\psi$ the angle between the $y$-axis and the radius vector. Then

$$r^2 = y^2(1 + \tan^2 \psi) .$$

With

$$z^2 = y^2 \tan^2 \psi = \frac{t^2}{4}[1 - (1 - 2x)^2 - (y/s)^2]$$

we obtain

$$r = \{1 - (1 - 2x)^2\}^{1/2} \left\{\frac{1 + \tan^2 \psi}{\left(\frac{1}{s}\right)^2 + \frac{\tan^2 \psi}{t^2/4}}\right\}^{1/2}$$

$$= \frac{\{1 - (1 - 2x)^2\}^{1/2}}{2\left\{\frac{\cos^2 \psi}{4s^2} + \frac{\sin^2 \psi}{t^2}\right\}^{1/2}}$$

$$\frac{dr}{dx} = \frac{1 - 2x}{\{1 - (1 - 2x)^2\}^{1/2}} \frac{1}{\left\{\frac{\cos^2 \psi}{4s^2} + \frac{\sin^2 \psi}{t^2}\right\}^{1/2}} . \qquad (100)$$

By equations (96) and (100):

$$V[x,y,z(x,y)] = \frac{V[x = 0 \cdot 5,y,z(0 \cdot 5,y)]}{\left\{1 + \left(\frac{dr}{dx}\right)^2\right\}^{1/2}} . \qquad (101)$$

In particular for the centre section, $y = 0$:

$$V[x,0,z(x,0)] = \frac{V[x = 0 \cdot 5,0,z(0 \cdot 5,0)]}{\left\{1 + \left(\frac{dz}{dx}\right)^2\right\}^{1/2}} . \qquad (102)$$

Velocity increments at the mid-chord point of the centre-section calculated by the various methods are plotted in Figs. 12 and 13 as function of the aspect ratio $A = 8s/\pi$. The parameter $t/2s$, used in the figures, characterises the spanwise slenderness of a cross-section, which decides if the simplifications of linear theory are permissible. The figures show that for very small aspect ratio the results from slender-body theory agree with the exact results and that linearised slender-body theory and linear theory give the same answer, as is to be expected. With the same aspect ratio, slender-body theory gives a better result for thin bodies, *i.e.*, small values of $t/2s$. Whereas for the axially symmetrical ellipsoid with $2s/c = 0 \cdot 4$ slender-body theory is in error by 40 per cent. For the flatter ellipsoid with $t/2s = 0 \cdot 2$, $2s/c = 0 \cdot 4$ it is wrong by only 15 per cent. We may, however, conclude that for wings with $t/2s > 0 \cdot 2$ the range of validity of the slender-body theory for determining thickness effects may be restricted to smaller aspect ratios than the corresponding theory of R. T. Jones[19] (1946) for lift effects. The spanwise fineness ratio is more favourable on tapered wings than on untapered wings of the same aspect ratio. We can therefore expect that slender-body theory is applicable to tapered wings of higher aspect ratio than untapered wings.

The discrepancies between linear and exact theory increase of course with the parameter $t/2s$. The figure shows that for $t/2s = 0 \cdot 2$ linear theory gives a result which is about 10 per cent too large for the whole aspect ratio range up to $1 \cdot 0$. Since $t/2s = 0 \cdot 2$ is a fairly large value for most practical wings, this result gives much confidence in the velocities calculated by linear theory at the centre-section of a wing.

10. *Conclusions.*—From theoretical considerations of thick wings at zero lift, the following conclusions may be drawn, regarding the effect of the aspect ratio on the pressure distribution:

(*a*) The principal effect of finite aspect ratio on the velocity distribution at the centre-section of rectangular wings is to reduce the velocity increments. The velocity distributions of wings of any section shape can be calculated in a short time by equations (10) and (46), using the coefficients given in Table 1.

(*b*) The effect of thickness taper on the velocity distribution at the centre-section of rectangular wings is again to reduce the velocity increments. With a thickness distribution decreasing linearly along the span, the velocity at the centre is decreased by an amount of the order $\frac{1}{8}\delta A v(A = \infty)$, where $\partial z/\partial |y| = -\delta z(x,y = 0)$. The velocity distribution can be calculated by equations (27) and (46), using the coefficients given in Tables 1 and 2.

(*c*) At the centre-section of swept wings, the velocity level is again reduced but less than on unswept wings; there may even be an increase of the velocity in some cases of highly swept-back wings. The position of the maximum velocity is generally farther forward on the wing with small aspect ratio than on the infinite wing. The effect of finite aspect ratio on the velocity distribution at the centre-section of untapered swept wings of any given section shape can be calculated by equations (37) and (46), using the coefficients given in Tables 3 and 4.

(*d*) In the special case of ellipsoidal wings with $t/c = 0 \cdot 1$, the results from linear theory are a fair approximation to the exact results for all aspect ratios. Slender-body theory gives sufficiently accurate results only if the aspect ratio is very small, smaller than $0 \cdot 5$, say. Linearised slender-body theory (Keune-Oswatitsch) happens to give reasonable results up to slightly higher aspect ratios, below $0 \cdot 8$, say.

---

## LIST OF SYMBOLS

| | | |
|---|---|---|
| $x,y,z$ | | Rectangular co-ordinates, $x$ in the direction of the main stream, $y$ spanwise, $z$ normal to the chordal plane, $x = 0$ at the leading edge |
| $x_\nu$, $x_\mu$ | | Position of fixed pivotal points (*see* Table 3 in Ref. 1) |
| $\zeta$ | = | $y + iz$, complex co-ordinate in a plane $x$ = constant |
| $\zeta_1$ | | Complex co-ordinate in the transformed $\zeta$-plane, where the body cross-section is transformed into a circle |
| $\zeta_1$ | = | $re^{i\theta}$, equation of the circle in the $\zeta_1$-plane |
| $\zeta_2$ | = | $y_2 + iz_2$, complex co-ordinate in the transformed $\zeta$-plane, where the body cross-section is transformed into a slit |
| $c$ | | Wing chord |
| $\bar{c}$ | | Mean wing chord |
| $s$ | | Half the wing span |
| $t$ | | Maximum thickness |
| $x_{\max}$ | | Position of maximum thickness |
| $z(x)$ | | Section shape |
| $z_\mu$ | = | $z(x_\mu)$, ordinate at $x = x_\mu$. |

| | | |
|---|---|---|
| $\delta$ | = | $-\dfrac{\partial}{\partial \lvert y \rvert}\left(\dfrac{z(x,y)}{z(x,0)}\right)$, thickness taper |
| $A$ | = | $\dfrac{2s}{\bar{c}}$, aspect ratio |
| $S(x)$ | | Cross sectional area in a plane $x =$ constant. |
| $\varphi$ | | Angle of sweep |
| $\varphi_{\mathrm{LE}}$ | | Sweep of leading edge |
| $V$ | | Total local velocity |
| $V_0$ | | Velocity of main stream |
| $V_{\max}$ | | Maximum velocity |
| $v_x$, $v_y$, $v_z$ | | Velocity increments in direction of the axes |
| $v_n$ | | Velocity component normal to the boundary of the body cross-section in a plane $x =$ constant. |
| $M_0$ | | Free-stream Mach number |
| $\beta$ | = | $(1 - M_0^{\,2})^{1/2}$ |
| $\phi$ | | Three-dimensional velocity potential |
| $\phi_1$ | | Two-dimensional velocity potential |
| $\phi_2$ | | *See* equations (61) and (72) |
| $q(x)$ | | Local strength of source distribution |
| $Q(x)$ | | Local strength of three-dimensional source distribution |
| $f(\varphi)$ | = | $\dfrac{1}{\pi}\ln\dfrac{1 + \sin\varphi}{1 - \sin\varphi}$ |
| $\vartheta$ | = | $\cos^{-1}(2x - 1)$ |
| $\vartheta_\nu$ | = | $\dfrac{\nu\pi}{N}$ |
| $\nu$ | | Suffix indicating the pivotal point |
| $\mu$ | | Suffix indicating the inducing point |
| $N$ | | Number of points taken along chord |
| $S^{(1)}(x_\nu)$ | = | $\sum_{\mu=1}^{N-1} s_{\mu\nu}^{(1)} z_\mu$, *see* equation (6) |
| $S^{(2)}(x_\nu)$ | = | $\sum_{\mu=1}^{N-1} s_{\mu\nu}^{(2)} z_\mu = \left(\dfrac{dz}{dx}\right)_{x=x_\nu}$ |
| $s_{\mu\nu}^{(1)}$ | | Coefficients, *see* Tables 4, 7 and 10 in Ref. 1 |
| $s_{\mu\nu}^{(2)}$ | | Coefficients, *see* Tables 5, 8 and 11 in Ref. 1 |
| $s_{\mu\nu}^{(6)}$ | | Coefficients, *see* Tables 1, 3 and 4 in this report |
| $s_{\mu\nu}^{(8)}$ | | Coefficients, *see* Table 2 in this report |

## REFERENCES


| No. | Author | Title, etc. |
|---|---|---|
| 1. | J. Weber .. .. .. .. | The calculation of the pressure distribution over the surface of two-dimensional and swept wings with symmetrical aerofoil sections. R. & M. 2918. July, 1953. |
| 2. | D. Küchemann and J. Weber .. | The subsonic flow past swept wings at zero lift without and with body. R. & M. 2908. March, 1953. |
| 3. | S. Neumark and J. Collingbourne | Velocity distribution on untapered sheared and swept-back wings of small thickness and finite aspect ratio at zero incidence. R. & M. 2717. March, 1949. |
| 4. | S. Neumark and J. Collingbourne | Velocity distribution on thin tapered wings with fore-and-aft symmetry and spanwise constant thickness ratio at zero incidence. R. & M. 2858. June, 1951. |
| 5. | K. W. Newby .. .. .. | The effects of taper on the supervelocities on three-dimensional wings at zero incidence. R.A.E. Report Aero. 2544. June, 1955. |
| 6. | O. Holme and F. Hjelte .. | On the calculation of the pressure distribution on three-dimensional wings at zero incidence in incompressible flow. K.T.H. Aero. Tech. Note 23. November, 1952. |
| 7. | J. Weber .. .. .. .. | An analysis of pressure measurements on delta wings in subsonic flow at zero incidence. R.A.E. Tech. Note Aero. 2032. A.R.C. 13,104. January, 1950. |
| 8. | M. C. Adams and W. R. Sears .. | Slender-body theory. Review and extension. *J. Ae. Sci.* Vol. 20, p. 85. 1953. |
| 9. | F. Keune .. .. .. .. | Low aspect ratio wings with small thickness at zero lift in subsonic and supersonic flow. K.T.H. Aero. Tech. Note 21. June, 1952. |
| 10. | J. Weber .. .. .. .. | Low-speed measurements of the pressure distribution near the tips of swept-back wings at no lift. R.A.E. Report Aero. 2318. A.R.C. 12,421. March, 1949. |
| 11. | J. Weber .. .. .. .. | Low-speed measurements of the pressure distributions and overall forces on wings of small aspect ratio and 53-deg sweepback. R.A.E. Tech. Note Aero. 2017. A.R.C. 12,878. September, 1949. |
| 12. | B. Göthert .. .. .. | Ebene und raümliche Strömung bei hohen Unterschallgeschwindigkeiten. Jahrb. 1941 d. deutschen Luftfahrtforschung, I p. 156. |
| 13. | H. Ludwieg .. .. .. | Improvement on the critical Mach number of aerofoils by sweepback. M.A.P. Völkenrode, Report and Translation No. 84. A.R.C. 9826. 1946. |
| 14. | F. Keune and K. Oswatitsch .. | Nicht angestellte Körper kleiner Spannweite in Unter-und Überschall-strömung. *Z.F.W.* Vol. 1, p. 137. 1953. |
| 15. | H. Lamb .. .. .. .. | *Hydrodynamics.* P. 152. Sixth edition. Cambridge University Press. 1932. |
| 16. | K. Maruhn .. .. .. | Druckverteilungsrechnungen an elliptischen Rümpfen und in ihrem Aussenraum. Jahrb. 1941 d. deutschen Luftfahrtforschung, I p. 135. |
| 17. | F. Keune .. .. .. .. | On the subsonic, transonic and supersonic flow around low aspect ratio wings with incidence and thickness. K.T.H. Aero. Tech. Note 28. September, 1953. |
| 18. | W. Gröbner, M. Hofreiter, N. Hofreiter, J. Laub and E. Peschl. | Table of integrals. Luftfahrtforschungsanstalt Braunschweig. 1944. TIB/MISC/873. |
| 19. | R. T. Jones .. .. .. | Properties of low-aspect-ratio pointed wings at speeds below and above the speed of sound. N.A.C.A. Report 835. 1946. |

## APPENDIX

*Approximation of Certain Integrals by Finite Sums*

The notation of Ref. 1 is used.

It was shown in Ref. 1, section 6, that by approximating $z(x)$ by an interpolation function

$$z(\vartheta) = \frac{2}{N} \sum_{\mu=1}^{N-1} z(x_\mu) \sum_{\lambda=1}^{N-1} \sin \lambda\vartheta_\mu \sin \lambda\vartheta \qquad \text{(A–1)}$$

with

$$\cos \vartheta = 2x - 1 \qquad \text{(A–2)}$$

the following relation holds:

$$\frac{1}{\pi}\int_0^1 \frac{dz(x')}{dx'} \frac{dx'}{x_\nu - x'} = \sum_{\mu=1}^{N-1} s_{\mu\nu}^{(1)} z(x_\mu) \qquad \text{(A–3)}$$

where

$$s_{\mu\nu}^{(1)} = \frac{(-1)^{\mu-\nu} - 1}{N} \frac{2 \sin \vartheta_\mu}{(\cos \vartheta_\mu - \cos \vartheta_\nu)^2}. \qquad \text{(A–4)}$$

Using the same interpolation function, an approximation for the integral

$$\frac{1}{\pi}\int_0^1 z(x') \frac{dx'}{x_\nu - x'}$$

can be obtained. By equations (6–1), (6–4), (6–38), (6–39), (6–41) and (6–11) of Ref. 1:

$$\begin{aligned}
\frac{1}{\pi}\int_0^1 z(x') \frac{dx'}{x_\nu - x'} &= \sum_{\mu=1}^{N-1} z(x_\mu) \cdot \frac{2}{\pi N} \sum_{\lambda=1}^{N-1} \sin \lambda\vartheta_\mu \int_0^\pi \frac{\sin \lambda\vartheta' \sin \vartheta' \, d\vartheta'}{\cos \vartheta_\nu - \cos \vartheta'} \\
&= \sum_{\mu=1}^{N-1} z(x_\mu) \cdot \frac{2}{N} \sum_{\lambda=1}^{N-1} \sin \lambda\vartheta_\mu \cos \lambda\vartheta_\nu \\
&= \sum_{\mu=1}^{N-1} z(x_\mu) \cdot \frac{\sin^2\vartheta_\mu}{2} [s_{\mu\nu}^{(1)} - s_{\mu\nu}^{(3)}] \\
&= \sum_{\mu=1}^{N-1} z(x_\mu) \frac{\cos \vartheta_\mu - \cos \vartheta_\nu}{2} s_{\mu\nu}^{(1)} \\
&= \sum_{\mu=1}^{N-1} s_{\mu\nu}^{(1)} (x_\mu - x_\nu) z(x_\mu). \qquad \text{(A–5)}
\end{aligned}$$

Applying the relations (A–3) and (A–5), the following general relation is obtained:

$$\begin{aligned}
\frac{1}{\pi}\int_0^1 \frac{dz(x')}{dx'} \frac{f(x')\, dx'}{x_\nu - x'} &= \frac{1}{\pi}\int_0^1 \frac{d(z(x') \,.\, f(x'))}{dx'} \frac{dx'}{x_\nu - x'} - \frac{1}{\pi}\int_0^1 z(x') \frac{df(x')}{dx'} \frac{dx'}{x_\nu - x'} \\
&= \sum_{\mu=1}^{N-1} s_{\mu\nu}^{(1)} \,.\, z(x_\mu) \,.\, f(x_\mu) - \sum_{\mu=1}^{N-1} s_{\mu\nu}^{(1)} (x_\mu - x_\nu) \,.\, z(x_\mu) \left(\frac{df(x)}{dx}\right)_{x_\mu} \\
&= \sum_{\mu=1}^{N-1} s_{\mu\nu}^{(1)} \left[ f(x_\mu) - (x_\mu - x_\nu) \left(\frac{df(x)}{dx}\right)_{x_\mu} \right] z(x_\mu). \qquad \text{(A–6)}
\end{aligned}$$

Deriving this relation two different interpolation functions (corresponding equation (A–1)) have been used, the first for $z(x) \,.\, f(x)$, the second for $z(x) \,.\, df(x)/dx$. Relation (A–5) can be used, when $f(x)$ and its derivative $df(x)/dx$ are finite continuous functions in the whole interval

$0 \leqslant x \leqslant 1$. When $f(x)$ or $df(x)/dx$ change rather rapidly somewhere in the interval, it will be necessary to take the values of $z(x) \, . \, f(x)$ or $z(x) \, . \, df/dx$ at a considerable number of points $x_\mu$ into account, to obtain a sufficient approximation.

To approximate integrals of the form

$$\frac{1}{\pi}\int_0^1 \frac{dz}{dx'}\, g(x')\, dx'$$

by finite sums, an interpolation formula for $z(x')\,\dfrac{dg(x')}{dx'}$ similar to (A–1) can be used:

$$\left(z(x')\,\frac{dg(x')}{dx'}\right) = \frac{2}{N}\sum_{\mu=1}^{N-1} z(x_\mu)\left(\frac{dg(x')}{dx'}\right)_{x'=x_\mu} \sum_{\lambda=1}^{N-1} \sin \lambda\vartheta_\mu \sin \lambda\vartheta \,. \quad \text{(A–7)}$$

The integral becomes :

$$\frac{1}{\pi}\int_0^1 \frac{dz}{dx'}\, g(x')\, dx' = \frac{1}{\pi}\Big[z(x')\,.\,g(x')\Big]_{x'=0}^{1} - \frac{1}{\pi}\int_0^1 z(x')\,\frac{dg(x')}{dx'}\, dx'$$

$$= -\frac{1}{\pi N}\sum_{\mu=1}^{N-1} z(x_\mu)\left(\frac{dg(x')}{dx'}\right)_{x'=x_\mu}\sum_{\lambda=1}^{N-1}\sin\lambda\vartheta_\mu \int_0^\pi \sin\lambda\vartheta' \sin\vartheta'\, d\vartheta'$$

$$= \sum_{\mu=1}^{N-1} -\frac{\sin\vartheta_\mu}{2N}\left(\frac{dg(x')}{dx'}\right)_{x'=x_\mu} z(x_\mu) \quad \text{(A–8)}$$

since

$$\int_0^\pi \sin\lambda\vartheta' \sin\vartheta'\, d\vartheta' = \begin{cases} \pi/2 & \text{for } \lambda = 1 \\ 0 & \text{for } \lambda \neq 1\,. \end{cases}$$

Another approximation for the integral can be found using equation (A–6).

$$\frac{1}{\pi}\int_0^1 \frac{dz}{dx'}\, g(x')\, dx' = \frac{1}{\pi}\int_0^1 \frac{dz}{dx'}\, g(x')(x_\nu - x')\,\frac{dx'}{x_\nu - x'}$$

$$= \sum_{\mu=1}^{N-1} s_{\mu\nu}^{(1)}\left[g(x_\mu)(x_\nu - x_\mu) + (x_\mu - x_\nu)^2\left(\frac{dg(x')}{dx'}\right)_{x'=x_\mu} + (x_\mu - x_\nu)g(x_\mu)\right] z(x_\mu)$$

$$= \sum s_{\mu\nu}^{(1)}(x_\mu - x_\nu)^2\left(\frac{dg(x')}{dx'}\right)_{x'=x_\mu} z(x_\mu)$$

$$= \sum_{\mu=1}^{N-1}\frac{(-1)^{\mu-\nu} - 1}{2N}\sin\vartheta_\mu\,.\left(\frac{dg(x')}{dx'}\right)_{x'=x_\mu} z(x_\mu) \quad \text{(A–9)}$$

The approximations (A–8) and (A–9) are of the same type. They differ due to the fact that interpolation formulae for different functions have been used, $z(x')\,\dfrac{dg(x')}{dx'}$ in equation (A–8); $z(x)\,.\,g(x')(x_\nu - x')$ and $z(x')\,\dfrac{d[g(x')(x_\nu - x')]}{dx'}$ in equation (A–9). The approximation (A–9) has the advantage that for the same $N$, i.e., the same degree of accuracy, only half the number of terms as compared with equation (A–8) have to be worked out.

TABLE 1

$$Coefficients\ s^{(6)}_{\mu\nu} = s^{(1)}_{\mu\nu}\left[1 - \frac{s\{2(x_\nu - x_\mu)^2 + s^2\}}{\{(x - x_\mu)^2 + s^2\}^{3/2}}\right]$$

$\varphi = 0,\ \gamma = 0;\ N = 8$

$s = 2{\cdot}0$

| $\mu$ | $\nu$ | | | | | | | |
|---|---|---|---|---|---|---|---|---|
| | 1 | 2 | 3 | 4 | 5 | 6 | 7 | 8 |
| 1 | 0 | 0·006 | 0 | 0·005 | 0 | 0·004 | 0 | 0·004 |
| 2 | 0·011 | 0 | 0·011 | 0 | 0·009 | 0 | 0·008 | 0 |
| 3 | 0 | 0·014 | 0 | 0·014 | 0 | 0·012 | 0 | 0·011 |
| 4 | 0·014 | 0 | 0·015 | 0 | 0·015 | 0 | 0·014 | 0 |
| 5 | 0 | 0·012 | 0 | 0·014 | 0 | 0·014 | 0 | 0·014 |
| 6 | 0·008 | 0 | 0·009 | 0 | 0·011 | 0 | 0·012 | 0 |
| 7 | 0 | 0·004 | 0 | 0·005 | 0 | 0·006 | 0 | 0·005 |

$s = 1{\cdot}0$

| $\mu$ | $\nu$ | | | | | | | |
|---|---|---|---|---|---|---|---|---|
| | 1 | 2 | 3 | 4 | 5 | 6 | 7 | 8 |
| 1 | 0 | 0·023 | 0 | 0·015 | 0 | 0·006 | 0 | 0·003 |
| 2 | 0·043 | 0 | 0·042 | 0 | 0·024 | 0 | 0·011 | 0 |
| 3 | 0 | 0·055 | 0 | 0·053 | 0 | 0·031 | 0 | 0·021 |
| 4 | 0·040 | 0 | 0·058 | 0 | 0·058 | 0 | 0·040 | 0 |
| 5 | 0 | 0·031 | 0 | 0·053 | 0 | 0·055 | 0 | 0·047 |
| 6 | 0·011 | 0 | 0·024 | 0 | 0·042 | 0 | 0·043 | 0 |
| 7 | 0 | 0·006 | 0 | 0·015 | 0 | 0·023 | 0 | 0·024 |

$s = 0{\cdot}5$

| $\mu$ | $\nu$ | | | | | | | |
|---|---|---|---|---|---|---|---|---|
| | 1 | 2 | 3 | 4 | 5 | 6 | 7 | 8 |
| 1 | 0 | 0·086 | 0 | 0·016 | 0 | −0·007 | 0 | −0·009 |
| 2 | 0·159 | 0 | 0·140 | 0 | 0·013 | 0 | −0·013 | 0 |
| 3 | 0 | 0·183 | 0 | 0·168 | 0 | 0·017 | 0 | −0·007 |
| 4 | 0·043 | 0 | 0·182 | 0 | 0·182 | 0 | 0·043 | 0 |
| 5 | 0 | 0·017 | 0 | 0·168 | 0 | 0·183 | 0 | 0·104 |
| 6 | −0·013 | 0 | 0·013 | 0 | 0·140 | 0 | 0·159 | 0 |
| 7 | 0 | −0·007 | 0 | 0·016 | 0 | 0·086 | 0 | 0·094 |

TABLE 1—*continued*

$$\textit{Coefficients } s_{\mu\nu}^{(6)} = s_{\mu\nu}^{(1)} \left[ 1 - \frac{s\{2(x_\nu - x_\mu)^2 + s^2\}}{\{(x_\nu - x_\mu)^2 + s^2\}^{3/2}} \right]$$

$$\varphi = 0,\ y = 0;\ N = 16$$

$s = 0 \cdot 25$

| $\mu$ | $\nu$ | | | | | | | | | | | | | | | |
|---|---|---|---|---|---|---|---|---|---|---|---|---|---|---|---|---|
| | 1 | 2 | 3 | 4 | 5 | 6 | 7 | 8 | 9 | 10 | 11 | 12 | 13 | 14 | 15 | 16 |
| 1 | 0 | 0·096 | 0 | 0·052 | 0 | 0·003 | 0 | —0·009 | 0 | —0·009 | 0 | —0·008 | 0 | —0·007 | 0 | —0·006 |
| 2 | 0·186 | 0 | 0·177 | 0 | 0·062 | 0 | —0·008 | 0 | —0·019 | 0 | —0·017 | 0 | —0·015 | 0 | —0·013 | 0 |
| 3 | 0 | 0·257 | 0 | 0·242 | 0 | 0·053 | 0 | —0·021 | 0 | —0·028 | 0 | —0·024 | 0 | —0·021 | 0 | —0·020 |
| 4 | 0·188 | 0 | 0·308 | 0 | 0·289 | 0 | 0·038 | 0 | —0·031 | 0 | —0·035 | 0 | —0·031 | 0 | —0·028 | 0 |
| 5 | 0 | 0·135 | 0 | 0·340 | 0 | 0·323 | 0 | 0·026 | 0 | —0·039 | 0 | —0·041 | 0 | —0·037 | 0 | —0·036 |
| 6 | 0·012 | 0 | 0·087 | 0 | 0·359 | 0 | 0·340 | 0 | 0·020 | 0 | —0·043 | 0 | —0·046 | 0 | —0·044 | 0 |
| 7 | 0 | —0·023 | 0 | 0·053 | 0 | 0·360 | 0 | 0·353 | 0 | 0·021 | 0 | —0·043 | 0 | —0·049 | 0 | —0·049 |
| 8 | —0·048 | 0 | —0·038 | 0 | 0·031 | 0 | 0·360 | 0 | 0·360 | 0 | 0·031 | 0 | —0·038 | 0 | —0·048 | 0 |
| 9 | 0 | —0·049 | 0 | —0·043 | 0 | 0·021 | 0 | 0·353 | 0 | 0·360 | 0 | 0·053 | 0 | —0·023 | 0 | —0·035 |
| 10 | —0·044 | 0 | —0·046 | 0 | —0·043 | 0 | 0·020 | 0 | 0·340 | 0 | 0·359 | 0 | 0·087 | 0 | 0·012 | 0 |
| 11 | 0 | —0·037 | 0 | —0·041 | 0 | —0·039 | 0 | 0·026 | 0 | 0·323 | 0 | 0·340 | 0 | 0·135 | 0 | 0·081 |
| 12 | —0·028 | 0 | —0·031 | 0 | —0·035 | 0 | —0·031 | 0 | 0·038 | 0 | 0·289 | 0 | 0·308 | 0 | 0·188 | 0 |
| 13 | 0 | —0·021 | 0 | —0·024 | 0 | —0·028 | 0 | —0·021 | 0 | 0·053 | 0 | 0·242 | 0 | 0·257 | 0 | 0·217 |
| 14 | —0·013 | 0 | —0·015 | 0 | —0·017 | 0 | —0·019 | 0 | —0·008 | 0 | 0·062 | 0 | 0·177 | 0 | 0·186 | 0 |
| 15 | 0 | —0·007 | 0 | —0·008 | 0 | —0·009 | 0 | —0·009 | 0 | 0·003 | 0 | 0·052 | 0 | 0·096 | 0 | 0·085 |

TABLE 2

$$\text{Coefficients } s_{\mu\nu}^{(8)} = -\, s_{\mu\nu}^{(1)} \frac{s^2(x_\nu - x_\mu)^2}{\{(x_\nu - x_\mu)^2 + s^2\}^{3/2}}$$

$$\varphi = 0,\ y = 0;\ N = 8$$

$s = 2\cdot0$

| $\mu$ | $\nu$ | | | | | | | |
|---|---|---|---|---|---|---|---|---|
| | 1 | 2 | 3 | 4 | 5 | 6 | 7 | 8 |
| 1 | 0 | 0·024 | 0 | 0·022 | 0 | 0·019 | 0 | 0·018 |
| 2 | 0·044 | 0 | 0·044 | 0 | 0·040 | 0 | 0·035 | 0 |
| 3 | 0 | 0·057 | 0 | 0·057 | 0 | 0·052 | 0 | 0·049 |
| 4 | 0·058 | 0 | 0·062 | 0 | 0·062 | 0 | 0·058 | 0 |
| 5 | 0 | 0·052 | 0 | 0·057 | 0 | 0·057 | 0 | 0·056 |
| 6 | 0·035 | 0 | 0·044 | 0 | 0·044 | 0 | 0·044 | 0 |
| 7 | 0 | 0·019 | 0 | 0·022 | 0 | 0·024 | 0 | 0·024 |

$s = 1\cdot0$

| $\mu$ | $\nu$ | | | | | | | |
|---|---|---|---|---|---|---|---|---|
| | 1 | 2 | 3 | 4 | 5 | 6 | 7 | 8 |
| 1 | 0 | 0·047 | 0 | 0·036 | 0 | 0·022 | 0 | 0·018 |
| 2 | 0·087 | 0 | 0·086 | 0 | 0·060 | 0 | 0·041 | 0 |
| 3 | 0 | 0·111 | 0 | 0·109 | 0 | 0·078 | 0 | 0·064 |
| 4 | 0·094 | 0 | 0·119 | 0 | 0·119 | 0 | 0·094 | 0 |
| 5 | 0 | 0·078 | 0 | 0·109 | 0 | 0·111 | 0 | 0·101 |
| 6 | 0·041 | 0 | 0·060 | 0 | 0·086 | 0 | 0·087 | 0 |
| 7 | 0 | 0·022 | 0 | 0·036 | 0 | 0·047 | 0 | 0·048 |

$s = 0\cdot5$

| $\mu$ | $\nu$ | | | | | | | |
|---|---|---|---|---|---|---|---|---|
| | 1 | 2 | 3 | 4 | 5 | 6 | 7 | 8 |
| 1 | 0 | 0·089 | 0 | 0·038 | 0 | 0·014 | 0 | 0·009 |
| 2 | 0·164 | 0 | 0·152 | 0 | 0·055 | 0 | 0·025 | 0 |
| 3 | 0 | 0·199 | 0 | 0·188 | 0 | 0·071 | 0 | 0·047 |
| 4 | 0·099 | 0 | 0·204 | 0 | 0·204 | 0 | 0·099 | 0 |
| 5 | 0 | 0·071 | 0 | 0·188 | 0 | 0·199 | 0 | 0·142 |
| 6 | 0·025 | 0 | 0·055 | 0 | 0·152 | 0 | 0·164 | 0 |
| 7 | 0 | 0·014 | 0 | 0·038 | 0 | 0·089 | 0 | 0·095 |

TABLE 2—*continued*

$$\textit{Coefficients } s^{(8)}_{\mu\nu} = -\, s^{(1)}_{\mu\nu} \frac{s^2(x_\nu - x_\mu)^2}{\{(x_\nu - x_\mu)^2 + s^2\}^{3/2}}$$

$$\varphi = 0,\ y = 0;\ N = 16$$

$s = 0{\cdot}25$

| $\mu$ | $\nu$ | | | | | | | | | | | | | | | |
|---|---|---|---|---|---|---|---|---|---|---|---|---|---|---|---|---|
| | 1 | 2 | 3 | 4 | 5 | 6 | 7 | 8 | 9 | 10 | 11 | 12 | 13 | 14 | 15 | 16 |
| 1 | 0 | 0·048 | 0 | 0·033 | 0 | 0·013 | 0 | 0·005 | 0 | 0·002 | 0 | 0·001 | 0 | 0·001 | 0 | 0·001 |
| 2 | 0·094 | 0 | 0·090 | 0 | 0·050 | 0 | 0·017 | 0 | 0·006 | 0 | 0·003 | 0 | 0·002 | 0 | 0·001 | 0 |
| 3 | 0 | 0·130 | 0 | 0·128 | 0 | 0·057 | 0 | 0·019 | 0 | 0·008 | 0 | 0·004 | 0 | 0·003 | 0 | 0·003 |
| 4 | 0·119 | 0 | 0·163 | 0 | 0·154 | 0 | 0·060 | 0 | 0·020 | 0 | 0·009 | 0 | 0·005 | 0 | 0·004 | 0 |
| 5 | 0 | 0·109 | 0 | 0·181 | 0 | 0·177 | 0 | 0·062 | 0 | 0·022 | 0 | 0·010 | 0 | 0·007 | 0 | 0·006 |
| 6 | 0·061 | 0 | 0·095 | 0 | 0·196 | 0 | 0·190 | 0 | 0·065 | 0 | 0·024 | 0 | 0·013 | 0 | 0·009 | 0 |
| 7 | 0 | 0·044 | 0 | 0·084 | 0 | 0·201 | 0 | 0·198 | 0 | 0·069 | 0 | 0·028 | 0 | 0·017 | 0 | 0·014 |
| 8 | 0·023 | 0 | 0·034 | 0 | 0·075 | 0 | 0·202 | 0 | 0·202 | 0 | 0·075 | 0 | 0·034 | 0 | 0·023 | 0 |
| 9 | 0 | 0·017 | 0 | 0·028 | 0 | 0·069 | 0 | 0·198 | 0 | 0·201 | 0 | 0·084 | 0 | 0·044 | 0 | 0·036 |
| 10 | 0·009 | 0 | 0·013 | 0 | 0·024 | 0 | 0·065 | 0 | 0·190 | 0 | 0·196 | 0 | 0·095 | 0 | 0·061 | 0 |
| 11 | 0 | 0·007 | 0 | 0·010 | 0 | 0·022 | 0 | 0·062 | 0 | 0·177 | 0 | 0·181 | 0 | 0·109 | 0 | 0·087 |
| 12 | 0·004 | 0 | 0·005 | 0 | 0·009 | 0 | 0·020 | 0 | 0·060 | 0 | 0·154 | 0 | 0·163 | 0 | 0·119 | 0 |
| 13 | 0 | 0·003 | 0 | 0·004 | 0 | 0·008 | 0 | 0·019 | 0 | 0·057 | 0 | 0·128 | 0 | 0·130 | 0 | 0·117 |
| 14 | 0·001 | 0 | 0·002 | 0 | 0·003 | 0 | 0·006 | 0 | 0·017 | 0 | 0·050 | 0 | 0·090 | 0 | 0·094 | 0 |
| 15 | 0 | 0·001 | 0 | 0·001 | 0 | 0·002 | 0 | 0·005 | 0 | 0·013 | 0 | 0·033 | 0 | 0·048 | 0 | 0·049 |

TABLE 3

$$\textit{Coefficients } s_{\mu\nu}^{(6)} = s_{\mu\nu}^{(1)} \left[ 1 - \frac{s\{2 \cos^2 \varphi \,.\, (x_\nu - x_\mu)^2 - 1\cdot 5 \sin 2\varphi \,.\, (x_\nu - x_\mu) s + s^2\}}{\{\cos^2 \varphi \,.\, (x_\nu - x_\mu)^2 - \sin 2\varphi \,.\, (x_\nu - x_\mu) s + s^2\}^{3/2}} \right]$$

$$\varphi = 45 \text{ deg};\ y = 0;\ N = 8$$

$s = 1\cdot 0$

| $\mu$ | $\nu$ | | | | | | | |
|---|---|---|---|---|---|---|---|---|
| | 1 | 2 | 3 | 4 | 5 | 6 | 7 | 8 |
| 1 | 0 | —0·006 | 0 | —0·007 | 0 | —0·006 | 0 | —0·006 |
| 2 | —0·010 | 0 | —0·012 | 0 | —0·012 | 0 | —0·011 | 0 |
| 3 | 0 | —0·011 | 0 | —0·016 | 0 | —0·016 | 0 | —0·015 |
| 4 | 0·003 | 0 | —0·011 | 0 | —0·017 | 0 | —0·017 | 0 |
| 5 | 0 | 0·009 | 0 | —0·010 | 0 | —0·016 | 0 | —0·016 |
| 6 | 0·025 | 0 | 0·007 | 0 | —0·008 | 0 | —0·012 | 0 |
| 7 | 0 | 0·014 | 0 | 0·001 | 0 | —0·005 | 0 | —0·006 |

$s = 0\cdot 5$

| $\mu$ | $\nu$ | | | | | | | |
|---|---|---|---|---|---|---|---|---|
| | 1 | 2 | 3 | 4 | 5 | 6 | 7 | 8 |
| 1 | 0 | —0·027 | 0 | —0·023 | 0 | —0·016 | 0 | —0·014 |
| 2 | —0·028 | 0 | —0·050 | 0 | —0·039 | 0 | —0·030 | 0 |
| 3 | 0 | —0·020 | 0 | —0·065 | 0 | —0·051 | 0 | —0·044 |
| 4 | 0·183 | 0 | —0·009 | 0 | —0·070 | 0 | —0·059 | 0 |
| 5 | 0 | 0·212 | 0 | —0·065 | 0 | —0·065 | 0 | —0·062 |
| 6 | 0·143 | 0 | 0·162 | 0 | —0·015 | 0 | —0·050 | 0 |
| 7 | 0 | 0·078 | 0 | 0·068 | 0 | —0·015 | 0 | —0·025 |

TABLE 3—*continued*

$$\textit{Coefficients}\ s^{(6)}_{\mu\nu} = s^{(1)}_{\mu\nu}\left[1 - \frac{s\{2\cos^2\varphi\,.\,(x_\nu - x_\mu)^2 - 1\cdot 5\sin 2\varphi\,.\,(x_\nu - x_\mu)s + s^2\}}{\{\cos^2\varphi\,.\,(x_\nu - x_\mu)^2 - \sin 2\varphi\,.\,(x_\nu - x_\mu)s + s^2\}^{3/2}}\right]$$

$\varphi = 45$ deg, $y = 0$, $N = 16$

$s = 0\cdot25$

| $\mu$ | $\nu$ | | | | | | | | | | | | | | | |
|---|---|---|---|---|---|---|---|---|---|---|---|---|---|---|---|---|
| | 1 | 2 | 3 | 4 | 5 | 6 | 7 | 8 | 9 | 10 | 11 | 12 | 13 | 14 | 15 | 16 |
| 1 | 0 | −0·027 | 0 | −0·027 | 0 | −0·020 | 0 | −0·014 | 0 | −0·010 | 0 | −0·007 | 0 | −0·007 | 0 | −0·006 |
| 2 | −0·041 | 0 | −0·054 | 0 | −0·049 | 0 | −0·035 | 0 | −0·024 | 0 | −0·018 | 0 | −0·014 | 0 | −0·013 | 0 |
| 3 | 0 | −0·049 | 0 | −0·082 | 0 | −0·062 | 0 | −0·047 | 0 | −0·033 | 0 | −0·024 | 0 | −0·021 | 0 | −0·020 |
| 4 | 0·055 | 0 | −0·061 | 0 | −0·100 | 0 | −0·081 | 0 | −0·055 | 0 | −0·040 | 0 | −0·031 | 0 | −0·028 | 0 |
| 5 | 0 | 0·182 | 0 | −0·042 | 0 | −0·119 | 0 | −0·091 | 0 | −0·062 | 0 | −0·047 | 0 | −0·040 | 0 | −0·037 |
| 6 | 0·454 | 0 | 0·320 | 0 | −0·031 | 0 | −0·130 | 0 | −0·099 | 0 | −0·069 | 0 | −0·054 | 0 | −0·048 | 0 |
| 7 | 0 | 0·460 | 0 | 0·420 | 0 | −0·020 | 0 | −0·139 | 0 | −0·105 | 0 | −0·076 | 0 | −0·062 | 0 | −0·059 |
| 8 | 0·264 | 0 | 0·390 | 0 | 0·467 | 0 | −0·013 | 0 | −0·141 | 0 | −0·109 | 0 | −0·083 | 0 | −0·075 | 0 |
| 9 | 0 | 0·168 | 0 | 0·322 | 0 | 0·472 | 0 | −0·013 | 0 | −0·139 | 0 | −0·112 | 0 | −0·091 | 0 | −0·084 |
| 10 | 0·068 | 0 | 0·116 | 0 | 0·276 | 0 | 0·444 | 0 | −0·018 | 0 | −0·132 | 0 | −0·105 | 0 | −0·096 | 0 |
| 11 | 0 | 0·040 | 0 | 0·088 | 0 | 0·249 | 0 | 0·389 | 0 | −0·027 | 0 | −0·117 | 0 | −0·106 | 0 | −0·100 |
| 12 | 0·013 | 0 | 0·027 | 0 | 0·075 | 0 | 0·233 | 0 | 0·304 | 0 | −0·037 | 0 | −0·105 | 0 | −0·088 | 0 |
| 13 | 0 | 0·007 | 0 | 0·021 | 0 | 0·068 | 0 | 0·218 | 0 | 0·192 | 0 | −0·048 | 0 | −0·078 | 0 | −0·079 |
| 14 | 0·001 | 0 | 0·004 | 0 | 0·018 | 0 | 0·065 | 0 | 0·180 | 0 | 0·083 | 0 | −0·034 | 0 | −0·052 | 0 |
| 15 | 0 | 0 | 0 | 0·003 | 0 | 0·014 | 0 | 0·052 | 0 | 0·110 | 0 | 0·016 | 0 | −0·021 | 0 | −0·024 |

TABLE 4

$$\textit{Coefficients } s_{\mu\nu}^{(6)} = s_{\mu\nu}^{(1)}\left[1 - \frac{s\{2\cos^2\varphi\,.\,(x_\nu - x_\mu)^2 - 1\cdot5\sin 2\varphi\,.\,(x_\nu - x_\mu)s + s^2\}}{\{\cos^2\varphi\,.\,(x_\nu - x_\mu)^2 - \sin 2\varphi\,.\,(x_\nu - x_\mu)s + s^2\}^{3/2}}\right]$$

$\varphi = 60$ deg, $y = 0$; $N = 8$

$s = 1\cdot0$

| $\mu$ | $\nu$ | | | | | | | |
|---|---|---|---|---|---|---|---|---|
| | 1 | 2 | 3 | 4 | 5 | 6 | 7 | 8 |
| 1 | 0 | −0·007 | 0 | −0·006 | 0 | −0·005 | 0 | −0·004 |
| 2 | −0·015 | 0 | −0·013 | 0 | −0·010 | 0 | −0·009 | 0 |
| 3 | 0 | −0·020 | 0 | −0·016 | 0 | −0·013 | 0 | −0·012 |
| 4 | −0·024 | 0 | −0·021 | 0 | −0·018 | 0 | −0·015 | 0 |
| 5 | 0 | −0·022 | 0 | −0·019 | 0 | −0·017 | 0 | −0·015 |
| 6 | −0·017 | 0 | −0·017 | 0 | −0·015 | 0 | −0·013 | 0 |
| 7 | 0 | −0·009 | 0 | −0·009 | 0 | −0·008 | 0 | −0·007 |

$s = 0\cdot5$

| $\mu$ | $\nu$ | | | | | | | |
|---|---|---|---|---|---|---|---|---|
| | 1 | 2 | 3 | 4 | 5 | 6 | 7 | 8 |
| 1 | 0 | −0·027 | 0 | −0·018 | 0 | −0·013 | 0 | −0·011 |
| 2 | −0·061 | 0 | −0·046 | 0 | −0·031 | 0 | −0·023 | 0 |
| 3 | 0 | −0·084 | 0 | −0·058 | 0 | −0·040 | 0 | −0·035 |
| 4 | −0·086 | 0 | −0·093 | 0 | −0·063 | 0 | −0·047 | 0 |
| 5 | 0 | −0·059 | 0 | −0·086 | 0 | −0·061 | 0 | −0·051 |
| 6 | 0·088 | 0 | −0·045 | 0 | −0·064 | 0 | −0·049 | 0 |
| 7 | 0 | 0·048 | 0 | −0·033 | 0 | −0·033 | 0 | −0·029 |

TABLE 4—*continued*

$$Coefficients\ s_{\mu\nu}^{(6)} = s_{\mu\nu}^{(1)}\left[1 - \frac{s\{2\cos^2\varphi\ .\ (x_\nu - x_\mu)^2 - 1\cdot5\sin 2\varphi\ .\ (x_\nu - x_\mu)s + s^2\}}{\{\cos^2\varphi\ .\ (x_\nu - x_\mu)^2 - \sin 2\varphi\ .\ (x_\nu - x_\mu)s + s^2\}^{3/2}}\right]$$

$$\varphi = 60\ \text{deg},\ y = 0,\ N = 16$$

$s = 0\cdot25$

| $\mu$ | $\nu$ | | | | | | | | | | | | | | | |
|---|---|---|---|---|---|---|---|---|---|---|---|---|---|---|---|---|
| | 1 | 2 | 3 | 4 | 5 | 6 | 7 | 8 | 9 | 10 | 11 | 12 | 13 | 14 | 15 | 16 |
| 1 | 0 | −0·028 | 0 | −0·022 | 0 | −0·016 | 0 | −0·012 | 0 | −0·008 | 0 | −0·006 | 0 | −0·006 | 0 | −0·004 |
| 2 | −0·064 | 0 | −0·054 | 0 | −0·040 | 0 | −0·028 | 0 | −0·020 | 0 | −0·014 | 0 | −0·012 | 0 | −0·010 | 0 |
| 3 | 0 | −0·096 | 0 | −0·076 | 0 | −0·054 | 0 | −0·036 | 0 | −0·026 | 0 | −0·020 | 0 | −0·018 | 0 | −0·016 |
| 4 | −0·136 | 0 | −0·124 | 0 | −0·094 | 0 | −0·064 | 0 | −0·044 | 0 | −0·032 | 0 | −0·026 | 0 | −0·024 | 0 |
| 5 | 0 | −0·160 | 0 | −0·150 | 0 | −0·108 | 0 | −0·072 | 0 | −0·050 | 0 | −0·036 | 0 | −0·032 | 0 | −0·030 |
| 6 | −0·074 | 0 | −0·164 | 0 | −0·170 | 0 | −0·118 | 0 | −0·078 | 0 | −0·054 | 0 | −0·044 | 0 | −0·038 | 0 |
| 7 | 0 | 0·098 | 0 | −0·146 | 0 | −0·182 | 0 | −0·124 | 0 | −0·082 | 0 | −0·060 | 0 | −0·050 | 0 | −0·046 |
| 8 | 0·464 | 0 | 0·278 | 0 | −0·120 | 0 | −0·186 | 0 | −0·126 | 0 | −0·086 | 0 | −0·066 | 0 | −0·056 | 0 |
| 9 | 0 | 0·470 | 0 | 0·378 | 0 | −0·098 | 0 | −0·182 | 0 | −0·124 | 0 | −0·088 | 0 | −0·070 | 0 | −0·065 |
| 10 | 0·290 | 0 | 0·394 | 0 | 0·394 | 0 | −0·092 | 0 | −0·172 | 0 | −0·120 | 0 | −0·088 | 0 | −0·076 | 0 |
| 11 | 0 | 0·198 | 0 | 0·324 | 0 | 0·356 | 0 | −0·098 | 0 | −0·152 | 0 | −0·110 | 0 | −0·086 | 0 | −0·080 |
| 12 | 0·100 | 0 | 0·146 | 0 | 0·276 | 0 | 0·272 | 0 | −0·106 | 0 | −0·128 | 0 | −0·096 | 0 | −0·082 | 0 |
| 13 | 0 | 0·066 | 0 | 0·116 | 0 | 0·236 | 0 | 0·154 | 0 | −0·098 | 0 | −0·098 | 0 | −0·078 | 0 | −0·072 |
| 14 | 0·030 | 0 | 0·044 | 0 | 0·092 | 0 | 0·182 | 0 | 0·038 | 0 | −0·074 | 0 | −0·066 | 0 | −0·056 | 0 |
| 15 | 0 | 0·016 | 0 | 0·028 | 0 | 0·060 | 0 | 0·090 | 0 | −0·016 | 0 | −0·038 | 0 | −0·032 | 0 | −0·032 |

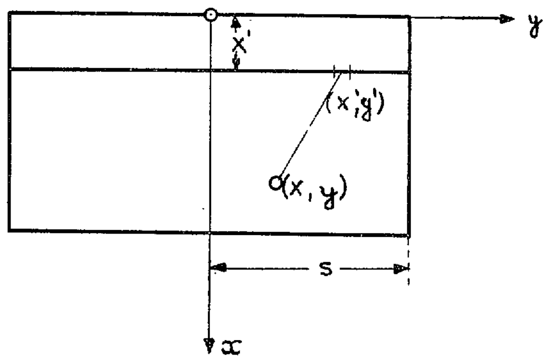


FIG. 1. Notation on straight wing.

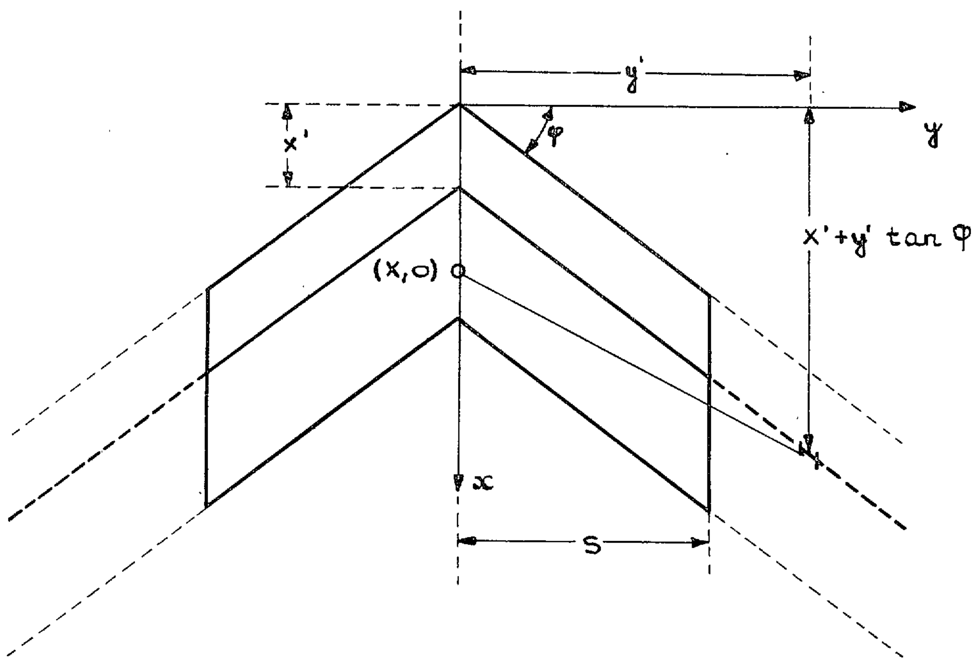


FIG. 2. Notation on swept wing.

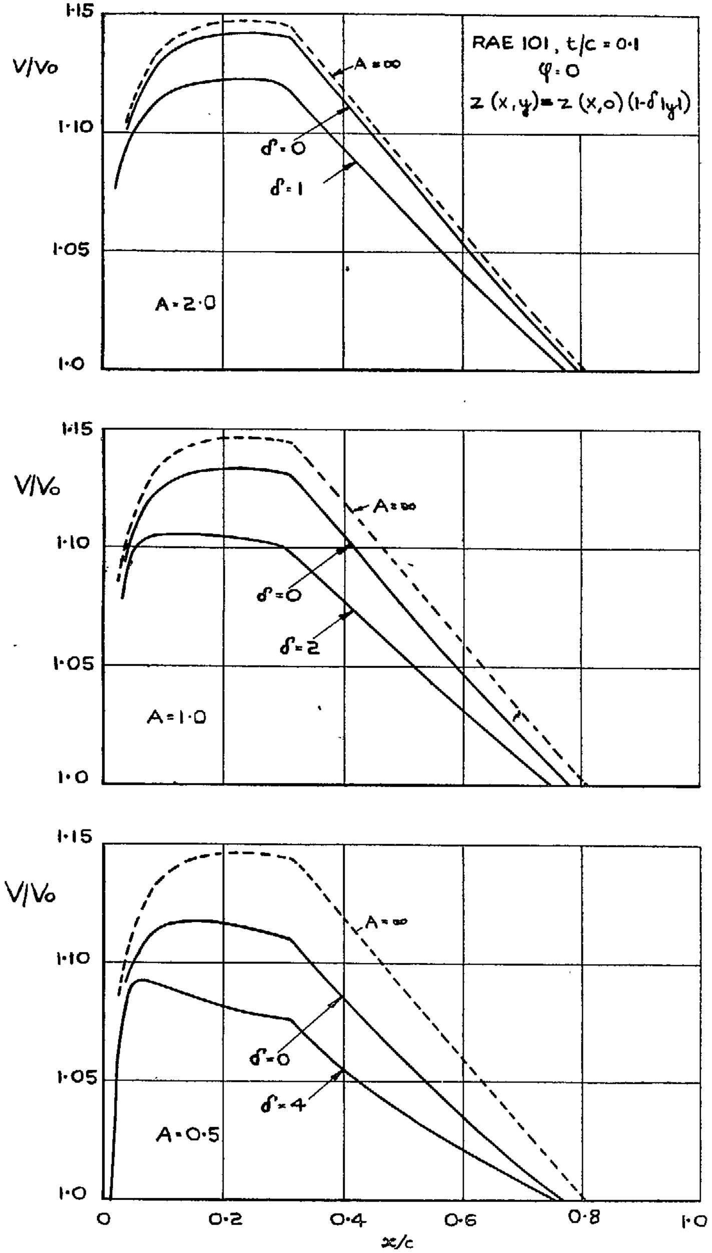


FIG. 3. Velocity distributions at the centre of straight wings.

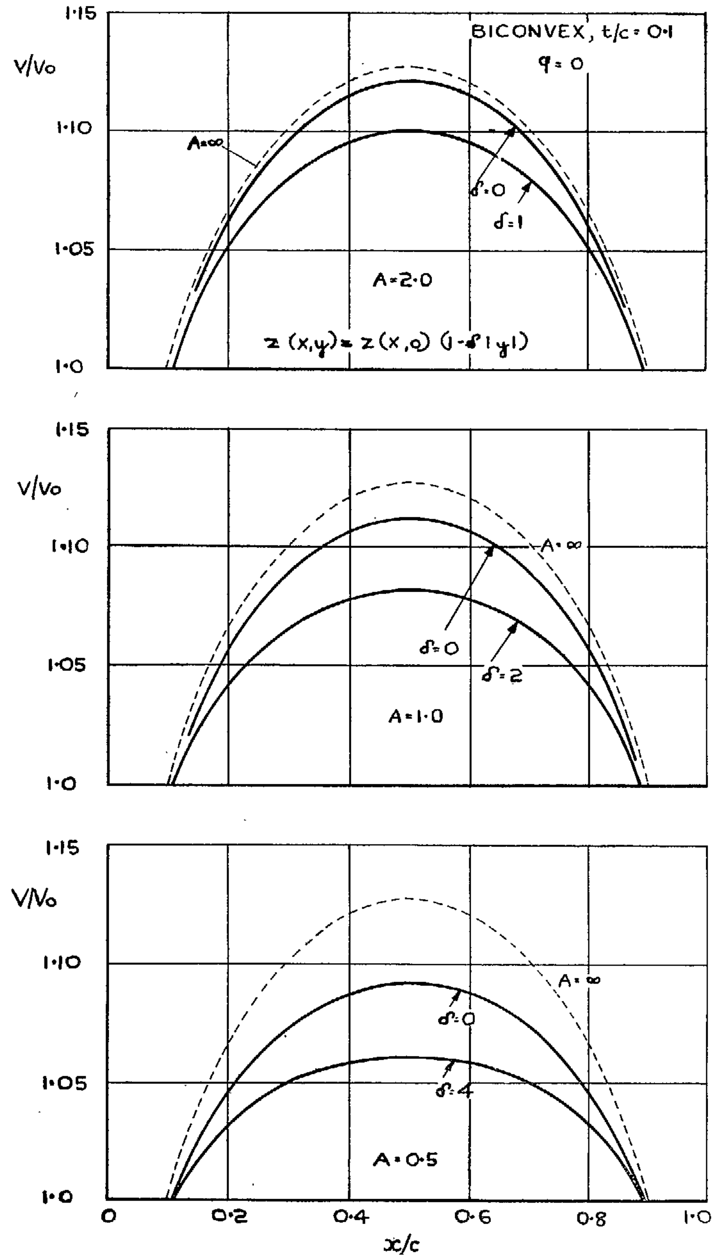


FIG. 4. Velocity distributions at the centre of straight wings.

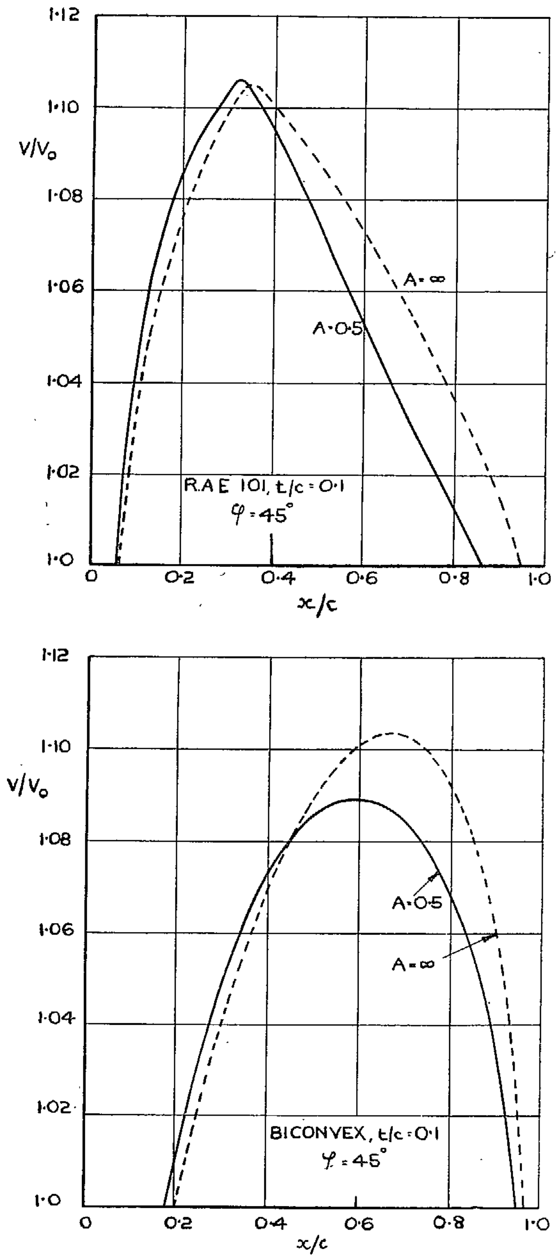


FIG. 5. Velocity distributions at the centre of swept wings.

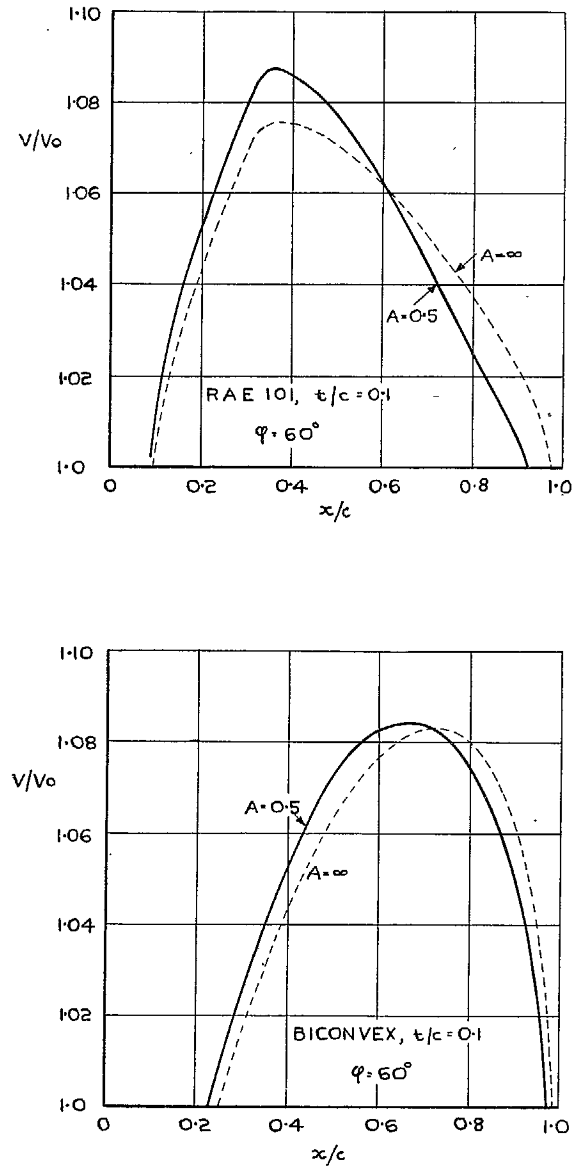


Fig. 6. Velocity distributions at the centre of swept wings.

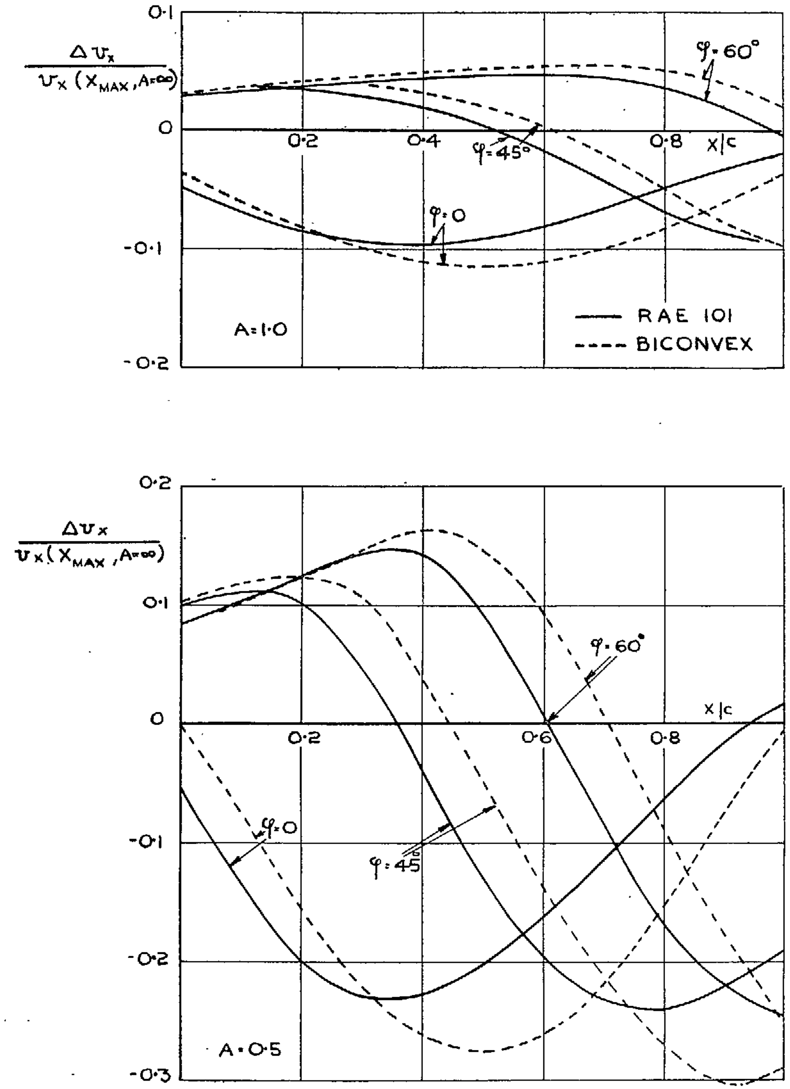


FIG. 7. Velocity increments.

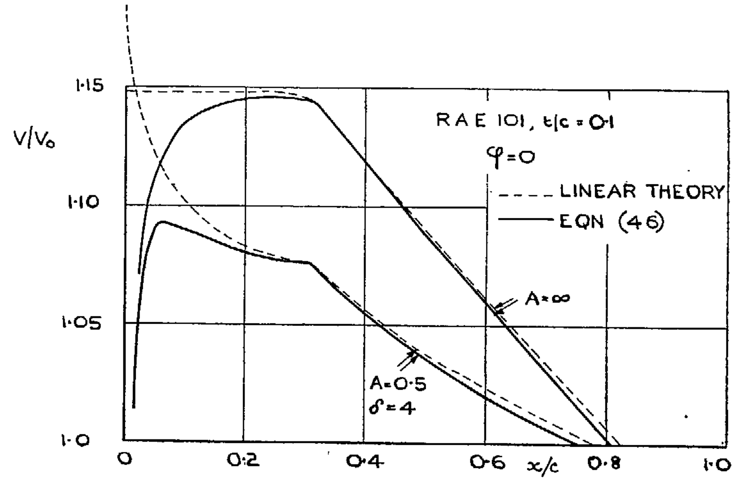


FIG. 8. Velocity distributions on straight wings.

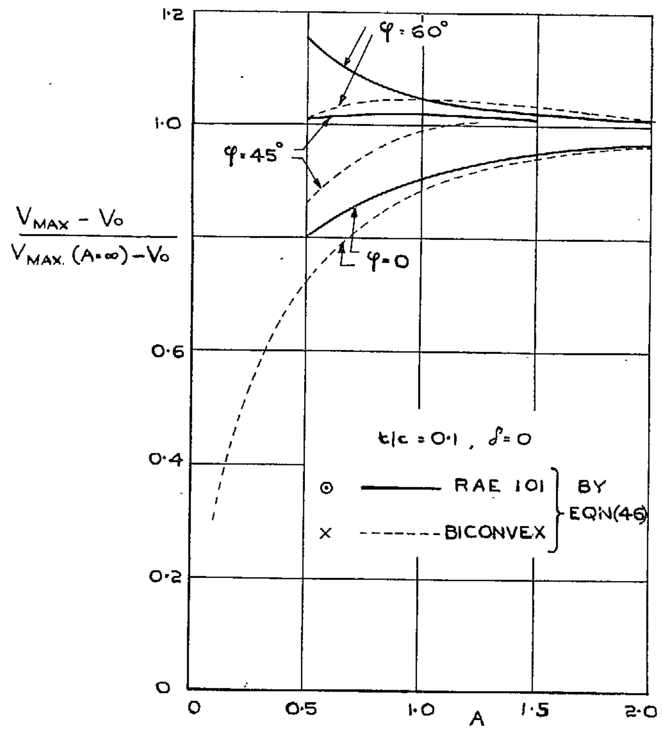


FIG. 9. Maximum velocities at the centre-section.

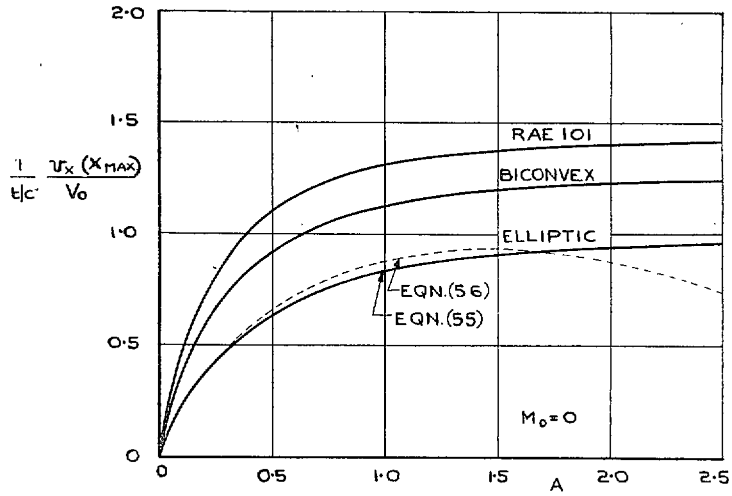


FIG. 10. Velocity increments at the maximum thickness position at the centre-section of rectangular wings.

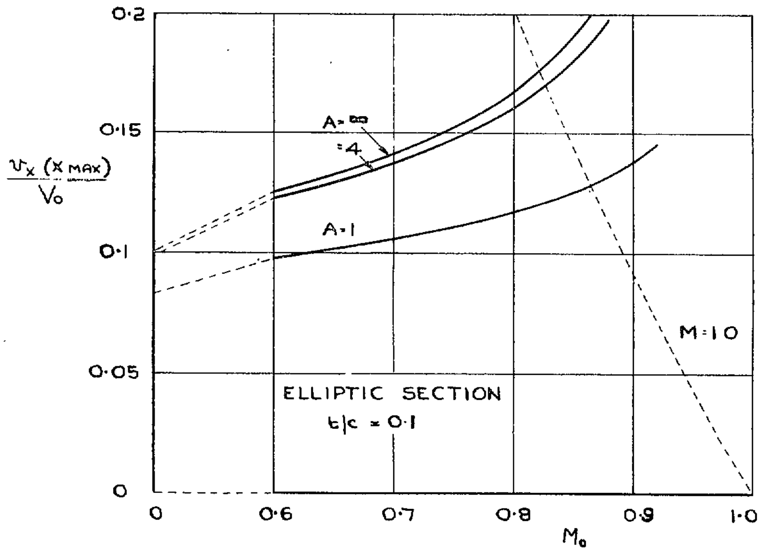


FIG. 11. Velocity rise with Mach number on rectangular wings.

(4578) Wt. 20 K.7 1/57 Hw.



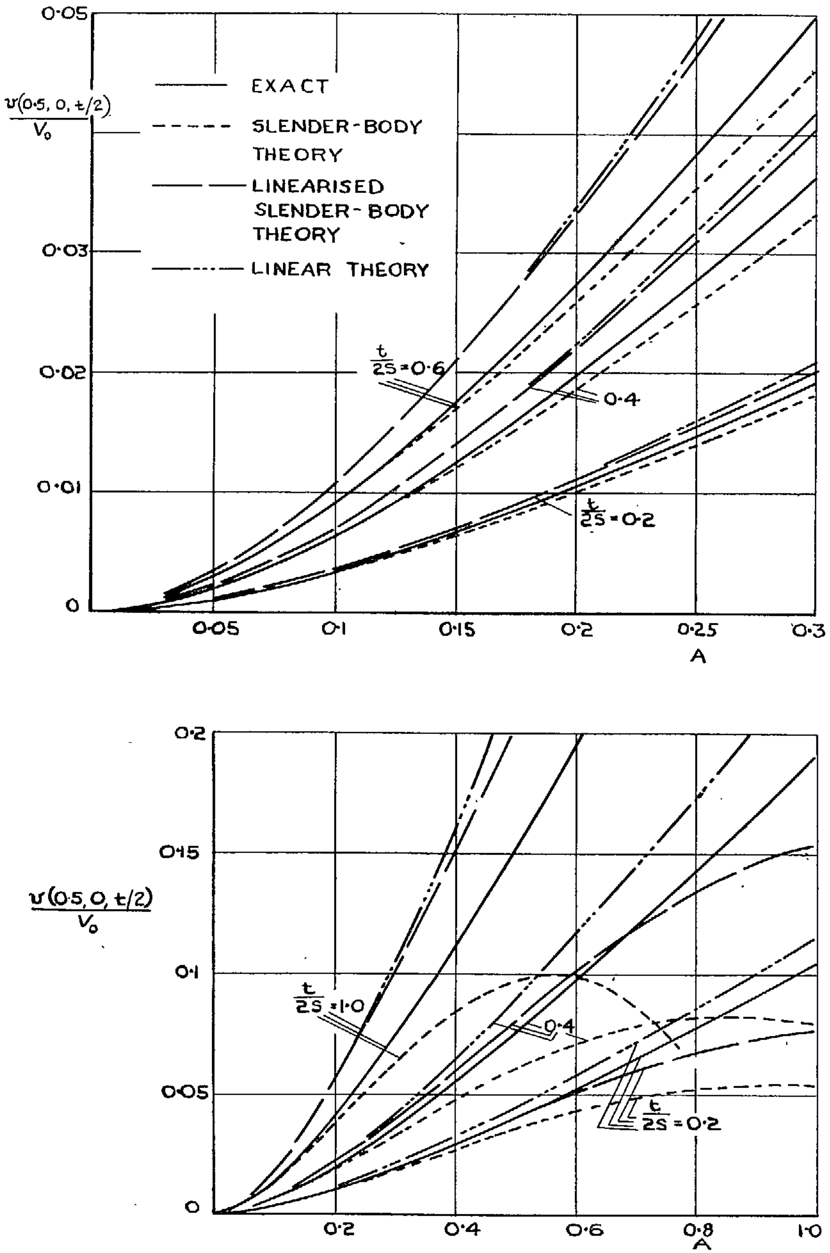


FIG. 12. Velocity increments on ellipsoids.

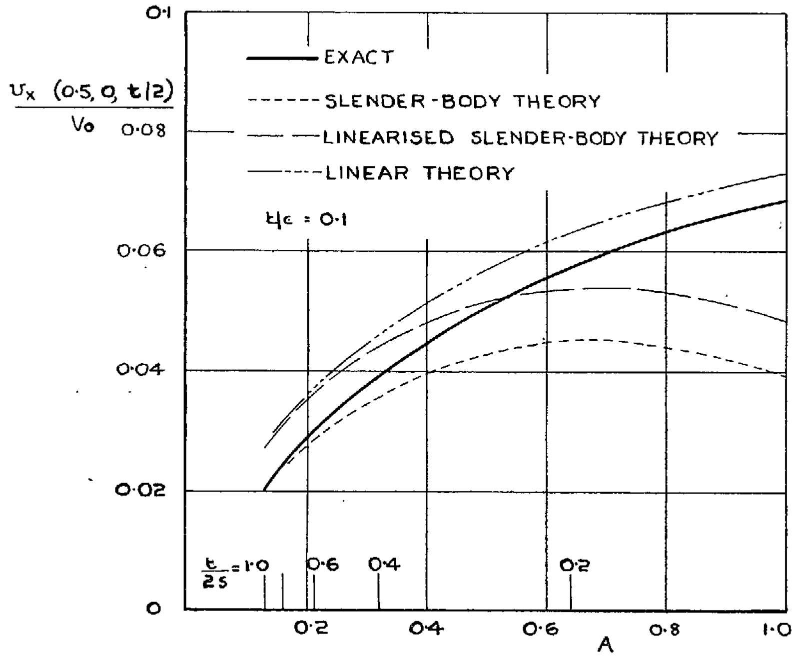


FIG. 13. Velocity increments on ellipsoids.

PRINTED IN GREAT BRITAIN

# Publications of the Aeronautical Research Council

## ANNUAL TECHNICAL REPORTS OF THE AERONAUTICAL RESEARCH COUNCIL (BOUND VOLUMES)

1939 Vol. I. Aerodynamics General, Performance, Airscrews, Engines. 50s. (51s. 9d.).
Vol. II. Stability and Control, Flutter and Vibration, Instruments, Structures, Seaplanes, etc. 63s. (64s. 9d.)

1940 Aero and Hydrodynamics, Aerofoils, Airscrews, Engines, Flutter, Icing, Stability and Control Structures, and a miscellaneous section. 50s. (51s. 9d.)

1941 Aero and Hydrodynamics, Aerofoils, Airscrews, Engines, Flutter, Stability and Control Structures. 63s. (64s. 9d.)

1942 Vol. I. Aero and Hydrodynamics, Aerofoils, Airscrews, Engines. 75s. (76s. 9d.)
Vol. II. Noise, Parachutes, Stability and Control, Structures, Vibration, Wind Tunnels. 47s. 6d. (49s. 3d.)

1943 Vol. I. Aerodynamics, Aerofoils, Airscrews. 80s. (81s. 9d.)
Vol. II. Engines, Flutter, Materials, Parachutes, Performance, Stability and Control, Structures. 90s. (92s. 6d.)

1944 Vol. I. Aero and Hydrodynamics, Aerofoils, Aircraft, Airscrews, Controls. 84s. (86s. 3d.)
Vol. II. Flutter and Vibration, Materials, Miscellaneous, Navigation, Parachutes, Performance, Plates and Panels, Stability, Structures, Test Equipment, Wind Tunnels. 84s. (86s. 3d.)

1945 Vol. I. Aero and Hydrodynamics, Aerofoils. 130s. (132s. 6d.)
Vol. II. Aircraft, Airscrews, Controls. 130s. (132s. 6d.)
Vol. III. Flutter and Vibration, Instruments, Miscellaneous, Parachutes, Plates and Panels, Propulsion. 130s. (132s. 3d.)
Vol. IV. Stability, Structures, Wind Tunnels, Wind Tunnel Technique. 130s. (132s. 3d.)

## Annual Reports of the Aeronautical Research Council—

1937 2s. (2s. 2d.) 1938 1s. 6d. (1s. 8d.) 1939–48 3s. (3s. 3d.)

## Index to all Reports and Memoranda published in the Annual Technical Reports, and separately—

April, 1950 - - - - - R. & M. 2600 2s. 6d. (2s. 8d.)

## Author Index to all Reports and Memoranda of the Aeronautical Research Council—

1909—January, 1954 R. & M. No. 2570 15s. (15s. 6d.)

## Indexes to the Technical Reports of the Aeronautical Research Council—

| | | |
|---|---|---|
| December 1, 1936—June 30, 1939 | R. & M. No. 1850 | 1s. 3d. (1s. 5d.) |
| July 1, 1939—June 30, 1945 | R. & M. No. 1950 | 1s. (1s. 2d.) |
| July 1, 1945—June 30, 1946 | R. & M. No. 2050 | 1s. (1s. 2d.) |
| July 1, 1946—December 31, 1946 | R. & M. No. 2150 | 1s. 3d. (1s. 5d.) |
| January 1, 1947—June 30, 1947 | R. & M. No. 2250 | 1s. 3d. (1s. 5d.) |

## Published Reports and Memoranda of the Aeronautical Research Council—

| | | |
|---|---|---|
| Between Nos. 2251–2349 | R. & M. No. 2350 | 1s. 9d. (1s. 11d.) |
| Between Nos. 2351–2449 | R. & M. No. 2450 | 2s. (2s. 2d.) |
| Between Nos. 2451–2549 | R. & M. No. 2550 | 2s. 6d. (2s. 8d.) |
| Between Nos. 2551–2649 | R. & M. No. 2650 | 2s. 6d. (2s. 8d.) |

*Prices in brackets include postage*

HER MAJESTY'S STATIONERY OFFICE

York House, Kingsway, London W.C.2; 423 Oxford Street, London W.1 (Post Orders: P.O. Box 569, London S.E.1) 13a Castle Street, Edinburgh 2; 39 King Street, Manchester 2; 2 Edmund Street, Birmingham 3; 109 St. Mary Street, Cardiff; Tower Lane, Bristol, 1; 80 Chichester Street, Belfast, *or through any bookseller.*

S.O. Code No. ~~23-2959~~ 23-2994